The ultrafast charge-transfer-to-solvent dynamics of iodide in tetrahydrofuran. 2. Photoinduced electron transfer to counterions in solution

Journal:	*The Journal of Physical Chemistry*
Manuscript ID:	jp-2007-12039u.R1
Manuscript Type:	Article
Date Submitted by the Author:	n/a

Complete List of Authors:	Bragg, Arthur; UCLA, Chem. & Biochem. Schwartz, Benjamin; University of California, Los Angeles, Chemistry and Biochemistry; The Journal of Physical Chemistry, Department of Chemistry and Biochemistry

The ultrafast charge-transfer-to-solvent dynamics of iodide in tetrahydrofuran. 2. Photoinduced electron transfer to counterions in solution

Arthur E. Bragg and Benjamin J. Schwartz*

Department of Chemistry and Biochemistry, University of California, Los Angeles, Los Angeles, California 90095-1569

Abstract: The excited states of atomic anions in liquids are bound only by the polarization of the surrounding solvent. Thus, the electron-detachment process following excitation to one of these solvent-bound states, known as charge-transfer-to-solvent (CTTS) states, provides a useful probe of solvent structure and dynamics. These transitions and subsequent relaxation dynamics also are influenced by other factors that alter the solution environment local to the CTTS anion, including the presence of cosolutes, cosolvents, and other ions. In this paper, we examine the ultrafast CTTS dynamics of iodide in liquid tetrahydrofuran (THF) with a particular focus on how the solvent dynamics and the CTTS electron-ejection process are altered in the presence of various counterions. In weakly-polar solvents such as THF, iodide salts can be strongly ion-paired in solution; the steady-state UV-visible absorption spectroscopy of various iodide salts in liquid THF indicates that the degree of ion-pairing changes from strong to weak to none as the counterion is switched from Na^+ to tetrabutylammonium ($t-BA^+$) to crown-ether-complexed Na^+, respectively. In our ultrafast experiments, we have excited the I^- CTTS transition of these various iodide salts at 263 nm and probed the dynamics of the CTTS-detached electrons throughout the visible and near-IR. In the previous paper of this series (A. E. Bragg and B. J. Schwartz, *J. Phys. Chem. B* **2008**, *112*, 483-494), we found that for 'counterion-free' I^- (obtained by complexing Na^+ with a crown ether) the CTTS electrons were ejected ~6 nm from their partner iodine atoms, the result of significant non-adiabatic coupling between the CTTS excited state and extended electronic states supported by the naturally existing solvent cavities in liquid THF, which also serve as pre-existing electron traps. In contrast, for the highly ion-paired NaI/THF

system, we find that ∼90% of the CTTS electrons are 'captured' by a nearby Na^+ to form $(Na^+, e^-)_{THF}$ tight-contact pairs (TCPs), which are chemically and spectroscopically distinct from both solvated neutral sodium atoms and free solvated electrons. A simple kinetic model is able to reproduce the details of the electron capture process, with 63% of the electrons captured quickly in ∼2.3 ps, 26% captured diffusively in ∼63 ps, and the remaining 11% escaping out into the solution on sub-ns time scales. We also find that the majority of the CTTS electrons are ejected to within 1 or 2 nm of the Na^+. This demonstrates that the presence of the nearby cation biases the relocalization of CTTS-generated electrons from I^- in THF, changing the non-adiabatic coupling to the extended, cavity-supported electronic states in THF to produce a much tighter distribution of electron-ejection distances. In the case of the more loosely ion-paired t−BA^+-I^-/THF system, we find that only 10-15% of the CTTS-ejected electrons associate with t−BA^+ to form 'loose-contact pairs' (LCPs), which are characterized by a much weaker interaction between the electron and cation than occurs in TCPs. The formation of $(t$−$BA^+, e^-)_{THF}$ LCPs is characterized by a coulombically induced blue-shift of the free e^-_{THF} spectrum on a ∼5-ps time scale. We argue that the weaker interaction between t−BA^+ and the parent I^- results in little change to the CTTS-ejection process, so that only those electrons that happen to localize in the vicinity of t−BA^+ are captured to form LCPs. Finally, we interpret the correlation between electron capture yield and counterion-induced perturbation of the I^- CTTS transition as arising from changes in the distribution of ion-pair separations with cation identity, and we discuss our results in the context of relevant salt conductivity measurements.

I. INTRODUCTION

Charge-transfer-to-solvent (CTTS) reactions of atomic anions are amongst the simplest solution-phase chemical reactions. These reactions are initiated by photoexcitation to bound solvent-supported excited states that do not exist for the bare ion in the gas phase.[1,2] Following excitation, these states relax as a result of solvent motions, leading to the generation

of a solvated electron, e^-_{solv}, and a solvated neutral atom:

$$X^- \xrightarrow{h\nu} X^{-*} \xrightarrow{CTTS} X + e^-_{\text{solv}}, \quad (1)$$

where X represents an atom whose excited anion, X^{-*}, can undergo a CTTS reaction in solution; these solvent-supported anionic excited states commonly are referred to as CTTS states. Because atomic anions lack intramolecular (nuclear) degrees of freedom, the dynamics of their photo-initiated CTTS reactions are dictated only by the solvent's structure and dynamic response to excitation. In turn, the solvent structure and response are strongly dependent on the molecular identity of the solvent, the ionic strength of the solution, and the presence of cosolutes and cosolvents. Consequently, CTTS reactions have a multivariate sensitivity to the local solution environment, and thus are ideal probes for investigating the microscopic dynamics of this environment and how these dynamics change with solution composition. In this paper, we use this sensitivity to explore how ion-pair interactions influence CTTS dynamics in weakly-polar solvents, specifically investigating how the CTTS dynamics of I^- in tetrahydrofuran (THF) are altered by the presence of salt counterions.

Since the advent of ultrafast laser sources, the CTTS reaction dynamics of several atomic anions in a variety of solvent environments have been examined in considerable detail.[1,3–15] For I^-, the CTTS dynamics in polar-protic[3] and polar-aprotic[6] environments are very similar. CTTS excitation of I^- in polar solvents leads to electron detachment near the partner I atom on a sub-100-fs time scale.[4–7] Subsequently, the nascent CTTS-ejected e^-_{solv} equilibrates with its local solution environment over several-to-tens of picoseconds, as evidenced by an initial dynamic blue-shift of the e^-_{solv}'s absorption spectrum.[5] After (and sometimes during) equilibration, the ejected electrons recombine with their geminate I-atom partners on a 10's-to-100's-of-ps time scale to regenerate the parent I^- ion.[3–5] Among polar solvents, differences in I^- CTTS dynamics originate from subtle differences in the dynamics of the solvent response, but do not reflect a qualitatively different picture of I^- CTTS.[16]

In contrast, the CTTS dynamics of I^- in weakly-polar, aprotic solvents can have a significantly different character. In previous work, we presented the wavelength- and time-dependent dynamics associated with the CTTS excitation of 'counterion-free' I^- in THF.[8] We found that THF-solvated electrons, e^-_{THF}, are ejected ∼380-fs following CTTS excitation and that the ejected electrons appear with their equilibrium absorption spectrum. Furthermore, we found that the ejected electrons do not undergo geminate recombination with

their I-atom partners on sub-nanosecond timescales. We also performed a series of competitive scavenging experiments that revealed a considerably larger spatial extent to the CTTS-excited state of I^- (and thus the initial electron-ejection distance) in THF relative to water. We interpreted these behaviors as resulting from the unusual liquid structure of THF: unlike most fluids, liquid THF packs poorly on the molecular level, resulting in a solvent structure characterized by a prevalence of electropositive solvent voids or cavities.[17,18] These cavities are natural traps for excess electrons and are also associated with low-lying, disjoint solvent-supported electronic excited states in THF that have amplitude in multiple cavities.[17] Excitation of an excess electron into these natural solvent-supported excited states can promote relocalization into cavities located up to nanometers away from the cavity of origin.[19,20] Thus, we assigned the large effective spatial extent (∼6 nm) of the I^- CTTS excited state in THF as originating from coupling between the local CTTS excited state and these low-lying disjoint solvent-supported electronic states.[8] Furthermore, we understand the lack of electron-solvation dynamics to reflect the fact that the solvent cavities in THF are nearly optimized to solvate an excess electron.[8] The CTTS excited state of I^- in water and other polar solvents, on the other hand, lies well below the conduction band,[5] and significant solvent rearrangement is required to solvate CTTS-generated solvated electrons, which localize close to the geminate I atom.

In studies of CTTS dynamics, the goal is usually to understand the properties of the 'free' CTTS system (*i.e.*, in the limit of infinite dilution) such that time-resolved measurements reflect only the influence of the solvent on the charge-transfer process. In aqueous solutions, this condition is achieved readily with monovalent salts at millimolar concentrations, as these salts typically dissolve to completion[21] and the high dielectric strength of water adequately screens ion-ion interactions (*i.e.*, the Onsager distance, r_c, at which coulombic attaction equals $k_{\mathrm{B}}T$, is on the order of a few Angstroms). On the other hand, these salts dissolve very poorly in weakly-polar solvents like THF ($K_{diss} \leq 10^{-5}$ M),[22] and ion-pair interactions are not screened even over relatively long distances (*i.e.*, r_c can be several nanometers). Thus, in order to investigate the dynamics of 'free' I^- in weakly polar solvents, it is necessary to screen coulombic interactions between salt counterions. In our previous study, we accomplished this by complexing Na^+ with 18-crown-6 cyclic ether.[8] Figure 1 illustrates that the I^- CTTS transition not only is affected by the polarity of the surrounding solvent medium (water vs. THF), but also is perturbed strongly by the presence of the nearby cation.[23] This figure

makes it clear that counterion-induced spectral shifts of the I^- CTTS band depend on the identity of the counterion: the absorption-band maximum of the 'free'-I^- CTTS transition lies at 254 nm (red squares), whereas that for tetrabutylammonium I^- and uncomplexed Na^+-I^- occur at 248 nm (green circles) and 236 nm (blue diamonds), respectively.[23] A similar scenario has been noted for alkali iodides in supercritical ammonia: steady-state absorption measurements indicate that these salts exhibit CTTS absorption from both 'free' and contact-pair species, and that the equilibrium between the 'free' and ion-paired species may be manipulated by altering the properties of the solvent.[24–27]

Given the strong counterion dependence of its CTTS absorption spectrum, how should we expect the dynamics of CTTS-excited iodide to change due to interactions with nearby charges? This issue has been addressed to some degree for aqueous ionic solutions. In high-dielectric liquids such as H_2O, raising the ionic strength generates increased *non-specific* ion-ion interactions that alter the hydration structure of CTTS anions and minimally perturb the CTTS (and $e^-_{H_2O}$) absorption spectrum.[2,28–30] Gelabert and Gaudel first invoked counterion stabilization of $e^-_{H_2O}$ and $e^-_{H_2O}$-Cl geminate pairs in an attempt to explain subtleties in the transient absorption dynamics that follow photodetachment of Cl^- in aqueous NaCl solutions.[31] However, it is unclear whether these small spectral perturbations are better assigned to specific interactions with a single Na^+ counterion than to non-specific interactions with a strong ionic atmosphere associated with the ∼1 M sample concentrations studied in these experiments.[31] In a more systematic study, Sauer *et al.*[29] showed that increasing the ionic strength can perturb the slow geminate recombination process that follows aqueous I^- CTTS excitation, such that the total free electron yield decreases with increased ionic strength. Yet, despite this subtlety, the CTTS dynamics of I^- in water were found to be qualitatively similar in solutions of varied ionic strength: locally ejected $e^-_{H_2O}$ either recombine with the geminate I atom or diffusively escape the weak attraction with the partner atom to become free electrons in solution.[29]

For I^- salts in THF, the sizeable shift of the I^- CTTS spectrum with counterion identity due to *specific* ion-pair interactions seen in Figure 1 portends considerable differences in CTTS dynamics with the identity of the dissolved salt — including the possibility of electron transfer to the counterion. With our understanding of the CTTS dynamics of 'free' iodide from our previous work,[8] we are now in a position to carefully examine how the presence of counterions alters the overall CTTS process. Our goal is to use ultrafast

spectroscopy to explore how the extent of ion-pairing and the proximity of countercations affects the CTTS dynamics of I^- in liquid THF. We ask specifically: do the counterions bias electron localization by altering the preexisting void structure and solvent-supported electronic states of THF? How does this affect the ejection distance of CTTS electrons in THF? Does ion pairing promote direct electron transfer to the counterion or induce new electron solvation dynamics? We will show that the presence of counterions affects not only the CTTS electron-ejection distribution, but also that proximal counterions can 'capture' the ejected electrons, forming either 'tight' or 'loose' cation:electron contact pairs that are spectroscopically distinct from 'free' solvated electrons. These spectroscopic differences provide a convenient handle with which we can assess cation-induced changes to the CTTS ejection dynamics. Moreover, the extensive ion-pairing of iodide salts in THF presents a useful starting point from which we can investigate electron-attachment dynamics in liquids in considerable detail.

The remainder of this paper is organized as follows. In Section II, we summarize our experimental methods, which have been described in more detail elsewhere.[8] Section III presents our time-resolved investigation of various I^- salts in liquid THF. We begin in Section III A by discussing the steady-state spectroscopy of the solvated electron and the various solvated electron:cation complexes that we generate through the photo-induced I^- CTTS reaction. In Section III B, we examine the CTTS dynamics of I^- in the presence of Na^+ using ultrafast transient absorption spectroscopy, and demonstrate that the CTTS excitation of I^- leads almost exclusively to the formation of $(Na^+, e^-)_{THF}$ tight-contact pairs. We also contrast the formation kinetics of $(Na^+, e^-)_{THF}$ with the geminate recombination dynamics that follow the CTTS excitation of counterion-free I^- in THF and the multiphoton ionization of neat THF in order to gauge the CTTS-generated distribution of electrons and cations. In Section III C, we illustrate that the CTTS excitation of I^- in the presence of tetrabutylammonium, $t{-}BA^+$, leads to formation of $(t{-}BA^+, e^-)_{THF}$ loose-contact pairs (LCPs). The dynamics associated with loose-contact pair formation are characterized by a subtle spectral shift of the absorption band of LCPs relative to 'free' THF-solvated electron. We analyze the wavelength-dependent transients with two different electron-capture models that enable us to extract the absorption spectrum of the $(t{-}BA^+, e^-)_{THF}$ loose-contact pair. We conclude in Section IV by discussing these results in the context of the thermodynamics of ion pairing, contrasting our measurements with conductivity data for THF-solvated salts

and comparing our measured cation-dependent electron-capture yields with cation-induced shifts in the CTTS spectra. The Appendix extensively describes the convolution methods we use to properly fold our experimental temporal response into our kinetic electron-capture models.

II. EXPERIMENTAL

The sample preparation and optical detection methods we use to investigate the time-resolved CTTS dynamics of I^- salts in THF have been described extensively in a recent publication.[8] Briefly, tetrahydrofuran (THF, Fischer) was dried over potassium metal under an Ar atmosphere and was distilled freshly for use; the freshly distilled solvent was optically transparent above ∼220 nm and was free of dissolved oxygen. Tetrabutylammonium ($(CH_3(CH_2)_3)_4N^+$) iodide, $t-BA^+$-I^- (Sigma, >99% purity), NaI (Fluka, >99.5% purity), and 18-crown-6 cyclic ether (1,4,7,10,13,16-hexa-oxa-cyclo-octa-decane, Aldrich, >98% purity) were used as purchased and were stored in a dessicator. Sample solutions (150-200 mL, 1-7.5 mM $t-BA^+$-I^-, 5-20 mM NaI) were prepared in a nitrogen drybox to curtail oxygen and water contamination, and were mixed via moderate sonication and/or modest heating in sealed flasks. Sample solutions were circulated through a 2-mm path length quartz flow cell (Spectrocell) using a peristaltic pump (Cole-Parmer); solutions flowed to the sample cell through a closed-circuit tubing loop that is chemically inert to both I^- and THF. The sample flow circuit was thoroughly flushed with nitrogen prior to sample introduction. Negligible sample oxidation occurred through the course of several hours, as verified both spectroscopically and according to the similarity of pump-probe data taken before and after several hours of exposing the samples to UV laser pulses. The spectroscopic signatures of various impurities (O_2, I_3^-, and H_2O) are well-understood,[32–34] such that we could easily identify contaminated samples. We used fresh solutions daily and replaced them in the event that the level of accumulated byproduct or contaminants became unacceptable.

Although we could not find published information regarding the solubility of these salts in THF, we note we were unable to prepare room-temperature solutions with $t-BA^+$-I^- concentrations above ∼10 mM even with extensive mixing, and that solutions with concentrations near 10 mM were stable only for a few hours. Most of our experiments using this salt were conducted with a 5-mM $t-BA^+$-I concentration in THF. In contrast, we were able

to make NaI solutions with concentrations up to 50 mM. Though a great deal of mixing was required to make solutions at these concentrations, we found that these solutions were indefinitely stable to precipitation. Since the 263-nm excitation wavelength we use in our experiments is at the very red edge of the Na^+-I^- CTTS transition (*cf.* Fig. 1), we conducted most of our experiments at a 20-mM NaI concentration in order to maximize absorption of the excitation light but avoid overly excessive sample concentrations. We did verify, however, that there was no concentration dependence of the NaI/THF CTTS dynamics down to the low mM concentration range.[35]

Our pump-probe transient absorption experiments were carried out using a regeneratively amplified Ti:sapphire laser (Spectra Physics) outputting ∼120-fs pulses centered near 790 nm (∼800-μJ pulse energy, 1-kHz repetition rate). Roughly one-third of of the amplified fundamental beam was frequency-tripled to generate 263-nm pump pulses with ∼3-5 μJ of energy in a two-stage 'doubling-mixing' scheme. The UV pulse intensity was controlled quantifiably with a set of calibrated, quartz-based neutral density filters. The remaining amplifier output was used to pump a dual-pass optical parametric amplifier (OPA, Spectra Physics), creating tunable signal and idler beams in the 1.2-2.5 μm range; for IR-probe experiments, these wavelengths were isolated and used directly. For near-IR- and visible-probe experiments, light pulses were produced either by doubling the signal or idler outputs (creating light in the 600-700 and 920-1100 nm ranges) or by sum-frequency generation (SFG) of either the signal or idler pulses with the remaining 790-nm fundamental light (creating light in the 470-650 nm range). Visible and near-IR-probe wavelengths were measured directly with an Ocean Optics fiber-based spectrometer at a ∼5-nm resolution, and the signal and idler wavelengths were measured according to the wavelength of SFG signal generated by mixing with the 790-nm fundamental. The relative pump-probe polarization was controlled for visible probe colors with a wave-plate/polarizer pair, and visible transients were collected with the relative pump and probe polarizations set at the magic angle (54.7°). We were unable to set the relative UV-IR polarization to the magic angle, but IR-probe transients recorded at both 0° and 90° relative polarization were identical across the range of investigated probe wavelengths.

The probe beam in our experiments was directed onto a computer-controlled, variable-delay translation stage (Newport) outfitted with a corner-cube reflector. The pump and probe beams were collinearly recombined using a 266-nm high reflector and were focused

towards the sample with a 100-mm fused-silica lens, with the sample placed 2-5 cm before the pump focus. The probe beam was collimated prior to recombination with a 1-m lens to ensure that the probe spot-size (∼50-100-μm diameter) was well within the pump spot-size (∼200-μm diameter). Visible absorption transients were measured with Si photodiodes (Thorlabs DET-100) and IR transients were recorded using either InGaAs photodiodes (Thorlabs DET-400) or InAs (Judson Technologies) photodetectors. A mechanical chopper was placed in the pump path to actuate pump-on/pump-off detection. A small portion of the probe beam was split off prior to the sample and was directed to a reference detector for shot-by-shot double normalization, whereby the intensity of the probe pulse transmitted through the sample is divided by the intensity measured on the reference detector both with and without the pump pulse present.[36] Each of the pump-probe transients presented here was collected by signal averaging for 30 min to 2 hours. All of the transients were collected at room temperature.

We close this section by discussing limitations to our temporal resolution induced by the nature of our samples. The volatility and hygroscopicity of THF precludes use of thin liquid sample jets that typically are employed to limit pump-probe refractive index mismatch (group velocity mismatch, GVM) in a liquid sample of finite width.[37] Although the refractive index of THF changes very little across the visible and near IR, the refractive index of THF increases significantly in the near UV due to pre-resonance with strong solvent absorption bands. We have measured a refractive index mismatch (Δn) of ∼0.2 between the 263-nm pump and IR-probe wavelengths in THF, corresponding to a ∼1.4-ps shift in time-zero upon passing both beams through 2 mm of the liquid.[38] This refractive-index mismatch through samples of finite width results in the convolution of 'true' absorption transients with the spatial variation of time-zero across the sample width, and typically introduces artifacts such as 'lazy' signal rises and broadened signal spikes that originate from coherent pump-probe interactions with the solvent. In fitting the models presented below, we have incorporated the effects of GVM by convolving the modelled dynamics with a sample response function that combines the refractive index mismatch with the sample-depth-dependent attenuation of the pump intensity. In the Appendix, we present the analytic result of this convolution for a multiexponential, time-dependent function and also include the effects of the pump-probe cross-correlation; we also describe a general numeric procedure for convolving these resolution effects (induced by GVM and finite pulse widths) with model functions exhibiting more complicated time-dependence.

III. THE EFFECTS OF COUNTERIONS ON THE CTTS DYNAMICS OF I^- IN THF

A. The steady-state spectroscopy of 'tight' and 'loose' cation:electron contact pairs in THF

It is generally accepted that solvated electrons exist as cavity-bound species in solution that have little valence interaction with surrounding solvent molecules. Figure 2 shows the spectrum of the THF-solvated electron (red squares[39–41]), and for reference, the spectrum of the hydrated electron (black curve[42]). The spectrum of the THF-solvated electron exhibits a broad absorption band that peaks in the IR at 2160 nm. Simulations have assigned this absorption spectrum as a superposition of the *s*-to-*p*-like transitions of a particle in a roughly spherical box at low energies and transitions between the *s*-like ground state and low-lying solvent disjoint states at higher energies.[17]

The spectroscopy of the solvated electron in weakly-polar solvents changes dramatically, however, in the presence of cations. For example, solvated electrons in ethers and amines are attracted to and captured by alkali cations in solution.[43–48] The spectrum of the species with stoichiometry Na^0, which is formed when solvated electrons associate with Na^+ in THF, spans the visible and near-IR, peaking at 870 nm (Fig. 2, blue diamonds).[43] The absorption band of this species is both substantially blue-shifted relative to the solvated electron's spectrum in THF and significantly red-shifted from the gas-phase sodium D-line (at 590 nm), suggesting that the chemical nature of this species lies somewhat between that of an unsolvated neutral atom and a solvated electron. In a recent investigation of the ultrafast CTTS dynamics of Na^- in THF, Cavanagh *et al.* demonstrated that this 870-nm band arises from a $(Na^+, e^-)_{THF}$ complex that is characterized by partial removal of the excess electron from the Na $3s$ orbital and thus is chemically distinct from a weakly solvated neutral sodium atom.[49] In this and future work,[50] we take advantage of the strong ion-pairing between Na^+ and I^- in liquid THF to directly probe the mechanisms by which the $(Na^+, e^-)_{THF}$ complex is formed from its constituent parts when Na^+ captures an excess electron generated by CTTS-excitation of a nearby I^- anion.

Although Na^+ in THF captures 100% of photo- or radiolytically generated electrons in solution, excess electrons in solutions made with solvents that interact more strongly with

Na^+, such as polyglycoldimethyl ethers (dimethoxy ether, diglyme, triglyme, etc.) are characterized by an equilibrium between 'strong' and 'weak' cation-electron interactions. Thus, electron injection into Na^+ solutions of polyglycoldimethyl ethers (glymes) yields two overlapping transient absorption bands: the first peaks near ∼900 nm, as with $(Na^+, e^-)_{THF}$, and the second is slightly blue-shifted from the e^-_{solv} spectrum in the absence of Na^+, peaking near ∼1600-1800 nm.[51,52] These two absorption bands are understood to originate from 'tight' and 'loose' electron:cation ion pairs in solution. Tight-contact pairs (TCPs), associated with the 870-nm band observed in THF, are characterized by substantial interaction of the electron with the outer *s*-orbital of the alkali cation, as evidenced by significant changes to the electron's hyperfine constant as measured via electron spin resonance (ESR).[53] On the other hand, loose-contact pairs (LCPs) are characterized by greater solvent separation and negligible valence interaction between the electron and the cation. The green dashed curve in Fig. 2 corresponds to the LCP spectrum in THF extracted from the measurements described in Section III C. The shift of the LCP spectrum relative to that of a free solvated electron arises largely as a perturbation by the attractive coulombic potential between the partners, and is presumed to be relatively insensitive to the cation identity.[51,52] We note that unlike the solvated electron:neutral atom contact pairs that are frequently invoked to explain CTTS recombination dynamics,[4,9] cation:electron TCPs and LCPs are spectroscopically distinct from the free e^-_{THF}. Thus, one of our goals in this work is to compare and contrast the formation of TCP and LCP species subsequent to the CTTS excitation of iodide.

B. Ultrafast CTTS dynamics of NaI in THF and the formation of $(Na^+, e^-)_{THF}$ tight-contact pairs.

1. *The capture of CTTS-ejected electrons by* Na^+

Because the electron-Na^+ interactions in THF are relatively well understood (*cf.* Fig. 2),[43,45] we begin our study of the effects of counterions on the CTTS dynamics of I^- in THF by examining the ultrafast spectroscopy of NaI/THF solutions. Figure 3 plots ultrafast absorption transients measured at representative infrared probe wavelengths following the 263-nm CTTS excitation of 20-mM NaI/THF solutions. For ease of comparison, we have normalized each of the transients at 25 ps, a time well after the fastest dynamical processes

are complete. The dynamics on longer time scales, $t < 500$ ps, are plotted in panels (a)-(g) (left), and the dynamics on early time scales, $t < 30$ ps, are shown on an expanded scale in panels (h)-(n) (right). The observed dynamics are clearly dependent on the probe wavelength. After an initial rise that we cannot resolve due to the pump-probe refractive-index mismatch (see Section II and the Appendix), the transient absorption intensity at 1670, 1440, 1270, and 1185 nm decays dramatically and the transient absorption measured at 700 and 920 nm exhibits an intensity rise on both ∼10- and ∼100-ps time scales; all of the transients reach a constant value by ∼300 ps. Additionally, we find a relatively flat temporal response when probing at 1080 nm at times > 30 ps (Fig. 3(l)), revealing a quasi-isosbestic point between the decaying long-wavelength and rising short-wavelength absorption transients.[54]

The NaI CTTS absorption transients plotted in Fig. 3 differ considerably from the those we measured previously following the CTTS excitation of 'counterion-free' I^- in THF.[8] Thus, the time- and wavelength-dependent transients of NaI/THF solutions highlighted in Fig. 3 must result from the participation of Na^+ in the CTTS kinetics. As our data strongly suggest two-state kinetics in which ejected electrons disappear to form a new species that absorbs farther to the blue, the logical conclusion is that the CTTS-ejected electrons are captured by proximal Na^+ cations in THF to form tight-contact pairs, $(Na^+, e^-)_{THF}$:

$$e^- + Na^+ \rightarrow (Na^+, e^-)_{THF}. \quad (2)$$

Indeed, the $(Na^+, e^-)_{THF}$ species has negligible absorption at wavelengths longer than ∼1400 nm (*cf.* Fig. 2), so that decaying absorption transients collected in this spectral window reflect changes in the population of the CTTS-ejected THF-solvated electrons. At wavelengths shorter than ∼1000 nm, the $(Na^+, e^-)_{THF}$ absorbs more strongly than the solvated electron, such that transients probed in this wavelength range primarily reflect TCP formation. Finally, the absorption spectra of THF-solvated electrons and $(Na^+, e^-)_{THF}$'s have equal cross-sections near 1080 nm (*cf.* Fig. 2), leading to quasi-isosbestic behavior at this probe wavelength.[54]

In order to support our assignment of the dynamics seen in Fig. 3 to the reaction of CTTS-generated electrons with Na^+ (Eq. 2) and to describe the transient behavior quantitatively, we introduce a kinetic capture model that utilizes the steady-state absorption spectroscopy

of $e^-_{\rm THF}$ and $(\rm Na^+, e^-)_{\rm THF}$:

$$\rm Na^+,\ I^- \xrightarrow{h\nu} Na^+,\ I^{-*} \tag{3a}$$

$$\rm Na^+,\ I^{-*} \xrightarrow{k_{CTTS}} Na^+,\ I,\ e^- \tag{3b}$$

$$\xrightarrow{k_f,\, f_f} (\rm Na^+, e^-)_{THF} \tag{3c}$$

$$\rm Na^+,\ e^- \xrightarrow{k_s,\, f_s} (Na^+, e^-)_{THF} \tag{3d}$$

$$\xrightarrow{f_{esc}} e^-_{\rm THF}. \tag{3e}$$

In this 'delayed-ejection-with-capture' scheme, electron ejection from the $\rm I^-$ CTTS excited state ($\rm I^{-*}$) occurs with rate k_{CTTS}. Following ejection, some of these electrons (which we assume have the free $e^-_{\rm THF}$ absorption spectrum plotted with red squares in Fig. 2) are captured by nearby $\rm Na^+$ to form $(\rm Na^+, e^-)_{THF}$ (with the equilibrium absorption spectrum plotted with blue diamonds in Fig. 2): a fraction f_f are captured on a fast time scale (with rate k_f), a fraction f_s are captured on a slow time scale (with rate k_s), and the remaining fraction $f_{esc} = 1 - f_f - f_s$ escape capture on sub-nanosecond time scales.[55] As described further below, the details of the capture processes depend not only on the initial distributon of parent $\rm Na^+$-$\rm I^-$ ion pairs, but also on the distribution of the CTTS-ejected electrons, as capture is driven by the relative diffusion of the electron and cation. Since we do not know either the initial proximity of the sodium and iodide ions or the precise nature of the electron-ejection distribution, we treat capture phenomenologically in this scheme with first-order kinetics (Eqs. 3c and 3d) to describe the ∼10- and ∼100-ps time scales apparent in the data in Fig. 3. As discussed more thouroughly below in Section III B 2, we presume that these two time scales correspond with the capture of electrons by closely- and further-separated $\rm Na^+$, respectively. Although we do not expect this simple capture model to reproduce all of the subtleties in the data, we will show that it does quantitatively explain most of the time and wavelength dependence of the NaI CTTS spectral transients plotted in Fig. 3.

In accordance with Eqn. 3, the time-dependent populations of electrons, $P_{e^-}(t)$, and $(\rm Na^+, e^-)_{THF}$ TCP species, $P_{(\rm Na^+, e^-)}(t)$, are given by

$$P_{e^-}(t) = f_{esc} + A_{CTTS}\exp\{-k_{CTTS}t\} + A_f\exp\{-k_ft\} + A_s\exp\{-k_st\},\ \text{ and,} \tag{4a}$$

$$P_{(\rm Na^+, e^-)}(t) = f_f + f_s - (1 + A_{CTTS})\exp\{-k_{CTTS}t\} - A_f\exp\{-k_ft\} - A_s\exp\{-k_st\}, \tag{4b}$$

in which

$$A_f = \frac{f_f k_{CTTS}}{k_{CTTS} - k_f} \text{ , } A_s = \frac{f_s k_{CTTS}}{k_{CTTS} - k_s} \text{ , and } A_{CTTS} = -(f_{esc} + A_f + A_s), \tag{5}$$

give the relative amplitudes of the different capture processes.[56] Thus, at any given probe wavelength λ, the transient absorption dynamics $I_\lambda(t)$ should directly reflect the population of each species weighted by its (equilibrium) absorption cross-section at that wavelength, $\epsilon_{\mathrm{X}}(\lambda)$:

$$I_\lambda(t) = \quad \epsilon_{e^-}(\lambda) \cdot P_{e^-}(t) + \epsilon_{(\mathrm{Na}^+,e^-)}(\lambda) \cdot P_{(\mathrm{Na}^+,e^-)}(t), \tag{6}$$

where X represents either the solvated electron or solvated sodium cation:electron TCP.

As described in Section II and the Appendix, the large group-velocity mismatch (GVM) between the UV-pump and IR-probe wavelengths through the finite width of the sample introduces an instrumental response that must be folded into our kinetic model in order to fit the data plotted in Fig. 3. This convolution introduces a dispersion-limited rise that obscures processes at times earlier than ∼1.4 ps. Since the electron-ejection time is clearly faster than our GVM-limited resolution, in our analysis, we fixed the electron-ejection time scale (k_{CTTS}^{-1}) to 380 fs, the value that we determined previously for 'free' iodide.[8] We note that the dispersion-limited rise precludes any observation of direct transfer of the CTTS-excited electron to the cation; therefore our analysis assumes that CTTS excitation always leads to electron ejection and that there is no direct charge-transfer to the cation (CTTC).[57] We justify this assumption further below in Section III B 2.

A global fit of Eqs. 4-6 to all seven of the NaI pump-probe transients is plotted as the solid black curves in Fig. 3; we used two adjustable rates (k_f and k_s) and capture yields (f_f and f_s) for a total of 4 fitting parameters. The best-fit parameters correspond to fast (k_f^{-1}) and slow (k_s^{-1}) capture processes that occur with 2.3 ± 0.6 and 63 ± 15 ps lifetimes, respectively, with the fast process (f_f) binding 63 ± 3% and the slow process (f_s) 26 ± 3% of the CTTS-generated electrons; 11% (f_{esc}) of the electrons remain uncaptured at $t = 500$ ps. The reported error bars reflect the range over which χ^2 increased by 25%. Figure 3 shows that the quality of the fit is excellent at both extremes of probed wavelength range. The relatively poor quality of the fit near 1100 nm (roughly the isosbestic point between e^-_{THF} and $(\mathrm{Na}^+, e^-)_{\mathrm{THF}}$; *cf.* Fig. 2) as well as the subtle differences at early delays at other wavelengths suggest that the kinetic-capture process involves spectral dynamics that are not included in

our model. We believe that these spectral dynamics likely include the formation of loosely-bound Na^+-electron LCPs prior to formation of the TCP as well as solvation/thermalization of the TCP immediately following electron capture.

2. *The effects of* Na^+ *on the CTTS ejection of electrons from* I^- *in THF*

Although our model provides a reasonable quantitative description of the $(Na^+, e^-)_{THF}$ formation kinetics that follow I^- CTTS excitation, how can we assess the degree to which the presence of a nearby sodium cation affects the CTTS electron-ejection process? Specifically, are CTTS electrons ejected to the same distance from the I atom in the presence and absence of Na^+? To address these questions, in Fig. 4 we examine pump-probe transients from both 'counterion-free' (*i.e.*, crown-ether-complexed Na^+; red squares) and Na^+-paired (blue diamonds) CTTS-excited I^- in THF collected by probing the population of free solvated electrons in the ~2-μm region; the data are normalized at $t = 10$ ps in order to highlight the slow relaxation processes. The red squares illustrate that negligible electron-I recombination follows the CTTS excitation of 'free' I^- in THF.[8] The curve through this data is the calculated electron survival probability assuming diffusive recombination via the Smoluchowski equation[58,59] with an initial 6-nm Gaussian-distributed pair separation. This calculation clarifies why so little recombination is observed up to 500 ps after excitation: the nascent CTTS-generated electrons from 'free' I^- are ejected far from their I-atom partners, a result consistent with our previous time-resolved scavenging experiments on this system.[8] In contrast, fitting of the transients plotted in Fig. 3 demonstrates that ~90% of the CTTS electrons ejected in NaI solutions are captured by Na^+ to make $(Na^+, e^-)_{THF}$ within ~300 ps. If the ejected electrons initially localize more than a few solvent shells from Na^+, then the dynamics of $(Na^+, e^-)_{THF}$ formation should be diffusion-controlled (subject to their screened coulombic attraction), much like the recombination of electrons and radical cations generated by solvent multiphoton ionization (MPI).[60–63] Therefore, the recombination kinetics of MPI-generated electrons/cations in THF can serve as a natural ruler against which we can estimate the initial relative spatial distribution of e^-_{THF}-Na^+ pairs associated with the slow recombination kinetics that follow CTTS excitation of Na^+-I^- in THF.

The electron recombination dynamics following MPI of neat THF through both visible[13] and ultraviolet[8] multiphoton excitation have been studied previously by our group, and in all

cases we were able to fit the observed recombination kinetics using an approximate solution to the Debye-Smoluchowski equation (DSE).[60,61] We found that when the multiphoton excitation provided ∼12.5 eV total energy, recombination is modelled reasonably by the DSE solution with a reaction distance $R = 11\pm1$ Å, a reaction velocity $v = 1.2\pm0.2$ m/s, and an initial electron ejection distance $r_0 \approx 40$ Å; for three-photon excitation at 263 nm, we found $r_0 = 37\pm2$ Å. The green circles in Fig. 4 plot the ∼2-μm-probed electron population kinetics following multiphoton ionization of neat THF at 263 nm, normalized at $t = 10$ ps; the solid green curve is a fit to the data with the approximate DSE solution, yielding the parameters stated above. The data illustrate that the recombination of solvated electrons with THF radical cations occurs on a *slower* time scale than the capture of solvated electrons by Na^+. Although we anticipate a similar mechanism for electron recombination following MPI and CTTS-electron capture by Na^+, one important difference distinguishes these processes: the initial electron-cation separation in MPI is determined simply by the excess energy available in the ionization process,[64] whereas the average e^--Na^+ interionic separation following CTTS excitation of Na^+-I^- results from a convolution of the ejected electron/I atom pair distribution with the equilibrium distribution of Na^+-I^- ion-pair separations. Thus, the diffusive capture of electrons by Na^+ following CTTS excitation of Na^+-I^- is truly a three-body problem, and to our knowledge, no general solution to this problem exists in the literature. The problem is further complicated by the fact that we expect the CTTS e^--ejection distribution to be affected significantly by the proximity of the sodium cation, such that there may be no unique combination of Na^+-I^- and electron-iodine distributions that generate the initial Na^+-e^- pair distribution.

How, then, can we estimate the average e^-_{THF}-cation separation following CTTS excitation of NaI in THF? One approach is to simply apply the approximate (two-body) DSE solution used for the MPI case to fit the slower of the two $(Na^+, e^-)_{THF}$ formation processes. The data are not sufficient to constrain the fit if all three DSE parameters are allowed to vary, but if we fix the reaction distance and velocity to be the same as those determined for recombination following MPI (11 Å and 1.2 m/s, respectively),[8,13] we obtain an initial cation-electron separation distance of 12 Å. Alternatively, if we fix only the reaction distance at 11 Å, we find that the slower electron-capture process can be described by the approximate DSE solution with an initial electron-cation separation of $\sim 24 \pm 3$ Å and with $v = 6 \pm 2$ m/s; this latter fit is plotted as the blue short-dashed curve through the NaI data in Fig. 4. Given

that there are no available published values for the reaction distance and velocity of solvated electrons interacting with Na^+ in THF and that there is no guarantee that the approximate solution to the DSE is appropriate for this three-body situation, the conclusion that we can draw from this approach is that the slower capture process, if diffusive, starts with an initial electron-Na^+ separation of roughly 1 to 2 nm.

We can support this number for the largest electron-Na^+ separation with a simple back-of-the-envelope calculation. To first order, the time scale for geminate electron-cation recombination can be approximated by the Onsager time $t_c = r_c^2/D'$, where r_c is the Onsager distance ($\sim$75 Å in THF) and D' is the relative diffusion constant for the diffusing electron/cation pair (0.76 Å^2/ps, assuming diffusion dominated by e^-_{THF});[65] for solvated electrons in THF, $t_c \approx 7.4$ ns. For the case of MPI, where we expect an initial separation distance $r_0 \approx 40$ Å between the electron and THF^+, we would expect the diffusive recombination time scale to be approximately

$$t_{40\text{Å}} \approx t_c \left[\frac{40\ \text{Å}}{r_c}\right]^2 \approx 2\ \text{ns}. \tag{7}$$

Figure 4 shows that roughly half of the recombination has occurred at the longest time probed (550 ps), such that this crude method provides a reasonable estimate of the time for recombination to be complete. In contrast, we see from the NaI transients in Fig. 3 that electron capture is complete by $\sim$300 ps. Since this time is much faster than the recombination time following MPI, we expect that the initial distribution of Na^+-e^-_{THF} distances must be considerably tighter than 40 Å. We thus can approximate roughly the initial electron-cation separation for the slow capture process as

$$r_0 \approx 75\ \text{Å}\sqrt{\frac{300\ \text{ps}}{7.4\ \text{ns}}} \approx 15\ \text{Å}. \tag{8}$$

Thus, this simple estimate gives a 1.5-nm initial separation distance for the CTTS-generated electrons and the sodium cations, in agreement with the DSE fit discussed above. Of course, this simple analysis relies on purely diffusive motions (without coulombic attraction) to bring the reactive pair together and also assumes that diffusion is dominated by e^-_{THF}; on both counts, we expect this analysis to somewhat underestimate the true initial pair separation.[66]

Despite the simplicity of these analyses, they do allow us to conclude with confidence that the initial separation between Na^+ and the CTTS-generated electrons is unlikely to be larger than $\sim$2 nm, particularly since more than 50% are captured by Na^+in 2.3 ps. It is therefore interesting to compare this $\leq$ 2-nm distance to the $\sim$6-nm electron-iodine separation that

we determined for the CTTS ejection of electrons from 'free' I^- in THF.[8] The fact that the two distances are so different indicates that the presence of proximal sodium cations has a profound influence on the CTTS-ejection process: electrons that would have been ejected nearly 6-nm away from their 'free' I atom parents are confined to be ejected well within ∼1-2 nm of the sodium counterion. Although the centers of these distributions do not coincide, we know from the CTTS spectroscopy and thermodynamics of these salts (see Section IV) that Na^+ cations are tightly ion-paired and likely reside within one or two solvent shells of the I^- ions. As a result, we anticipate that the distribution centers are not so different on the scale of the electron-ejection distance. Thus, even the electrons that are most slowly captured are not ejected more than ∼2 nm away from the I atom when the Na^+ cation is nearby, such that Na^+ induces a dramatic collapse of the CTTS electron-ejection distribution.

Of course, this analysis applies only to the longer of the two Na^+-electron capture processes from our kinetic model (the 63-ps process). The faster, 2.3-ps capture process is clearly too fast to be diffusion-limited, and thus must be rate-limited by the fluctuations of the THF molecules solvating the sodium cation. We presume that Na^+ not only is dipole-solvated by the surrounding THF molecules but also that Na^+-THF interactions involve some coordination of oxygen lone pairs to the bare cation (similar interactions as those between the cation and glymes,[51,52] but weaker since THF is only monodentate). We believe that this solvation structure presents a barrier for electron attachment that inhibits faster electron transfer. The right side of Figure 3 shows that the faster capture process is not well described by the simple two-state kinetic interconversion model expressed by Eqn. 2. This also points to the important role of solvent fluctuations and dynamic solvation in the faster capture process, with the implication that electron-Na^+ interactions evolve from free e^-_{THF} to $(Na^+, e^-)_{\mathrm{THF}}$ through one or more intermediate stages as the solvent reorganizes. On these grounds, we argue that direct, photoinduced charge-transfer between I^- and Na^+, a process that would compete with CTTS electron ejection, is highly unlikely: the solvent structure around Na^+ is simply too far from optimal to accomodate a tight-contact pair for direct charge-transfer to occur.[57] We will analyze the early-time portion of the NaI pump-probe transients in more detail in an upcoming paper with the goal of elucidating the spectral intermediates and dynamic solvation involved in the fast electron capture-process.[50]

C. CTTS dynamics of tetrabutylammonium iodide in tetrahydrofuran and the formation of $(t{-}\mathrm{BA}^+, e^-)_{\mathrm{THF}}$ 'loose-contact pairs.'

As described above, $(\mathrm{Na}^+, e^-)_{\mathrm{THF}}$ is characterized by a partially atomic binding interaction. What about cases in which electron-cation pairs are defined by weak interactions? Unlike the case of Na^+, we anticipate no valence interactions between the electron and $t{-}\mathrm{BA}^+$, which is characterized by long, alkyl arms and a filled valence shell on the central nitrogen atom. We also expect weaker ion-pairing between $t{-}\mathrm{BA}^+$ and I^-; indeed, Fig. 1 illustrates that the steady-state absorption spectrum of I^- is only weakly perturbed by the presence of tetrabutylammonium relative to the 'counterion-free' anion. This suggests that either $t{-}\mathrm{BA}^+$-I^- has an increased interionic separation or that tetrabutylammonium cannot induce a large inherent perturbation to the I^- CTTS spectrum relative to Na^+. In this section, we examine the CTTS dynamics of I^- in the presence of $t{-}\mathrm{BA}^+$ with the goal of using these dynamics to assess the strength of both $t{-}\mathrm{BA}^+$-electron and $t{-}\mathrm{BA}^+$-I^- interactions.

Figure 5 presents the ultrafast transient absorption dynamics of a 5-mM $t{-}\mathrm{BA}^+$-I^- solution in THF following CTTS excitation at 263 nm; the data are normalized at $t = 40$ ps and are offset for clarity. On long timescales (panel (a)), no wavelength dependence in the transient absorption is observed across the IR, and there is negligible decay of the absorption even up to 1 ns after excitation.[67] This wavelength independence and lack of any significant dynamics is similar to what we observed following excitation of 'free' I^- in THF.[8] The lack of any long-time wavelength dependence to the spectral dynamics differs significantly from the NaI system, however, and indicates that any role played by the $t{-}\mathrm{BA}^+$ cation in electron capture or on the CTTS ejection process is not particularly dramatic. However, we do observe a subtle wavelength dependence at early times (Fig. 5(b)): the transient absorption intensity shows a small decay at longer wavelengths (*e.g.*, 2300 nm, pink circles) and a small rise at shorter wavelengths (*e.g.*, 1375 nm, gray circles) in the first 10-15 ps following excitation. We also see (outside our GVM-limited rise) quasi-isosbestic character at intermediate wavelengths (*e.g.*, 1650/1750 nm, dark/light blue circles). These spectral dynamics are absent with 'counterion-free' I^- and must therefore reflect time-dependent $t{-}\mathrm{BA}^+$-e^- interactions.

What kind of $t{-}\mathrm{BA}^+$-electron interactions could be responsible for the dynamics seen in Fig. 5? As we described in Section III A, the spectrum of electron-cation LCPs in ethers

($\lambda_{max} \approx$ 1600-1800 nm) are somewhat blue-shifted relative to that of free solvated electrons ($\lambda_{max} \approx$ 1900-2100 nm). If we assume that electron capture by $t-\mathrm{BA}^+$ in THF leads to LCP formation, then the absorption intensity decrease at longer wavelengths signifies a reduction in the population of free solvated electrons as they are captured by the $t-\mathrm{BA}^+$ cation, while the concomitant absorption intensity increase at shorter wavelengths reflects the growth of newly formed LCPs. Unfortunately, we cannot quantitatively model these $t-\mathrm{BA}^+$-electron capture dynamics using the same kinetic scheme invoked in the previous section for electron capture by Na^+ because the equilibrium spectrum of the $t-\mathrm{BA}^+$-electron loose-contact pair has not been measured independently. We do know, however, that the oscillator strength of the electron's absorption spectrum should remain unchanged through the capture transformation $e^-_{\mathrm{THF}} \rightarrow (t-\mathrm{BA}^+, e^-)_{\mathrm{THF}}$, even though LCP formation might change the peak position and spectral shape. To simplify our analysis, we will assume that the equilibrium spectrum of $(t-\mathrm{BA}^+, e^-)_{\mathrm{THF}}$ has the same shape and oscillator strength as that of the free THF-solvated electron but with a blue-shifted peak wavelength, thereby introducing only one spectroscopic parameter (λ^{LCP}_{max}) into our kinetic modeling of the LCP capture process. Here, we use the same well-known Gaussian-Lorentzian lineshape to describe both the e^-_{THF} and $(t-\mathrm{BA}^+, e^-)_{\mathrm{THF}}$ equilibrium absorption bands.[68]

With this spectroscopic approximation in hand, we are now in a position to construct a kinetic model for electron capture by $t-\mathrm{BA}^+$ following the CTTS excitation of $t-\mathrm{BA}^+$-I^- in THF. As with the case of NaI, we could simply assume that the free solvated electron and captured contact pair are chemically distinct species and that the capture process is reasonably modeled by a simple first-order kinetic interconversion between them. On the other hand, we also could argue that $(t-\mathrm{BA}^+, e^-)_{\mathrm{THF}}$ is better thought of as a coulombically perturbed free solvated electron, so that the spectrum of the electron should shift smoothly to the blue as the electron-$t-\mathrm{BA}^+$ separation decreases. Since we do not know which picture of the electron-capture process makes the most physical sense, we have modelled the transients in Fig. 5 with kinetic schemes that describe both pictures. Our first scheme assumes a kinetic interconversion between e^-_{THF} and $(t-\mathrm{BA}^+, e^-)_{\mathrm{THF}}$ in a manner similar to Eq. 3, but using only a single interconversion rate (τ^{-1}) and branching ratio (f); we refer to this approach as the 'kinetic-capture' model. In this model, the spectra of e^-_{THF} and $(t-\mathrm{BA}^+, e^-)_{\mathrm{THF}}$ are assumed to be static, but λ^{LCP}_{max} is used as a fitting parameter. Our second scheme also invokes a single formation rate (τ^{-1}) and capture fraction (f), but

incorporates a continuous spectral blue-shift between free e^-_{THF} and $(t{-}\mathrm{BA}^+, e^-)_{\mathrm{THF}}$:

$$t{-}\mathrm{BA}^+ \; + e^-_{\mathrm{THF}} \; \overset{f,\tau,S(t,\lambda)}{\longrightarrow} (t{-}\mathrm{BA}^+, e^-)_{\mathrm{THF}}. \tag{9}$$

Here, $S(t,\lambda)$ represents a continuously shifting Gaussian-Lorentzian band whose parameters associated with the halfwidths are held constant, thereby fixing the band shape, but whose peak frequency shifts according to

$$\omega(t) = \omega^{LCP}_{max} + (\omega^{free}_{max} - \omega^{LCP}_{max}) \exp(-\frac{t}{\tau}), \tag{10}$$

where ω^{free}_{max} and ω^{LCP}_{max} are the initial and final peak frequencies, and τ is the spectral-shifting time scale. We refer to this scheme as the 'ionic-solvation' model. We note that convolution of the ionic-solvation model with our GVM-affected temporal response is not analytic and must be done numerically; our procedure for carrying out this numerical convolution is described in the Appendix. Importantly, both of our kinetic schemes incorporate only three adjustable parameters (f, τ, and λ^{LCP}_{max}), but with implicity different physics.

The non-linear least-squares fit of the ionic-solvation model to all of the $t{-}\mathrm{BA}^+$-I^- pump-probe data are plotted as the black curves in Fig. 5; the fit to the kinetic-capture model is indistinguishable from the fit to the ionic-solvation model and thus is not shown here. The parameters determined from the fits to both models are given in Table I; as with our fits for the NaI/THF pump-probe transients, the error bars for each parameter are determined by the range over which χ^2 increases by 25%. The fact that the two models yield virtually indistinguishable fits indicates that both can describe the data reasonably well, and Table I shows that both models yield identical fitting parameters within the estimated error. In particular, both models give λ^{max}_{LCP} as lying ~400-500 nm to the blue of the free e^-_{THF}, in excellent agreement with previous observations of LCPs seen in other solvents;[51,52] the $(t{-}\mathrm{BA}^+, e^-)_{\mathrm{THF}}$ spectrum determined by fitting our data with the ionic-solvation model is plotted as the green dashed curve in Fig. 2. Both models also suggest that only $f \approx$ 10-15% of the CTTS-generated electrons are captured by $t{-}\mathrm{BA}^+$ to form LCPs on a $\tau \approx$ 5-ps time scale.

We close this section by noting that the χ^2 and parameter error bars obtained by fitting the data with the ionic-solvation model are slightly smaller (though, not significantly smaller statistically) than those obtained by fitting with the kinetic-capture model. This suggests that the continuous blue-shift of the ionic-solvation model may more closely capture the dynamics that occur following CTTS excitation of $t{-}\mathrm{BA}^+$-I^- in THF than the kinetic-capture

	'ionic solvation'	'kinetic capture'
f_{attach}	0.135 ± 0.05	0.11 ± 0.045
λ_{LCP}^{max}	1695 ± 100 nm	1608 ± 150 nm
τ_{attach}	5.05 ps (2.5-9.5)	5.80 ps (2.5-13.5)
χ^2	0.36	0.41

TABLE I: Fitting parameters obtained applying the ionic-solvation and kinetic-capture models to $t-BA^+$-I^- transients plotted in FIG. 5.

model. Our intuition about the LCP-formation process likewise favors this mechanism. Of course, the true dynamic behavior may involve a combination of both types of processes, changes in the absorption bandshape that may occur during the LCP capture process, or even direct LCP formation from the CTTS excited state. Given that LCP formation leads only to subtle changes in the transient spectrocopy, the role of any of these additional processes would be difficult to assess from the data in Fig. 5, particularly since each of them would require the introduction of additional fitting parameters. Nevertheless, in contrast to both the NaI and 'counterion-free' I^- systems, our analysis clearly demonstrates the formation of LCPs with a perturbatively blue-shifted absorption spectrum following the CTTS excitation of $t-BA^+$-I^-.

IV. DISCUSSION: THE CORRELATION BETWEEN ION-PAIRING AND CTTS DYNAMICS

In the previous section, we examined the ultrafast dynamics following the CTTS excitation of I^- in THF associated with different counterions. We found that following CTTS excitation of NaI/THF solutions, ∼90% of the CTTS-generated electrons are captured by the sodium cations to form $(Na^+, e^-)_{THF}$ tight-contact pairs, as evident from the dramatic changes in the transient absorption in the near-IR (Fig. 3). We also found that following CTTS excitation of $t-BA^+$-I^- solutions in THF, only ∼10-15% of the ejected electrons are captured to form $(t-BA^+, e^-)_{THF}$ loose-contact pairs, as determined from the relatively subtle changes in the dynamic spectroscopy (Fig. 5). The dynamics in both cases differ from those of CTTS-excited 'counterion-free' I^- in THF (Fig. 4 and Ref. 8), for which there are no spectral dynamics following the initial electron ejection, indicating the absence of

electron-counterion and electron-iodine interactions (as well as observable electron-solvation dynamics). The data demonstrate that the the degree of electron capture correlates directly with the spectral shift of the I^- CTTS transition induced by the counterion (*cf.* Fig. 1). We believe that this correlation can be explained most generally in terms of a difference in the strength of ion-pair interactions between the precursor-salt counterions. The work of Blandamer *et al.*[23] and Sciaini *et al.*[24–27] suggests that the blue-shift of the I^- CTTS transition that results upon substituting $t-BA^+$ with Na^+ indicates a smaller average separation of the Na^+ counterion with the nearby I^- ion. Our previous work showed that the addition of 18-crown-6 ether breaks up Na^+-I^- ion pairs by better solvating the sodium cation, leading to a large red-shift of the CTTS spectrum.[8] Thus, the correlation we observe is that electron capture is more efficient when the cations are initially closer to the I^- ion (in which case the CTTS transition is more strongly perturbed) than when the cations are initially far from the I^- ion (in which case the CTTS transition has undergone little counterion-induced blueshift). In as much as the interionic separation reflects the nature of ion-pair types (contact, solvent-separated, etc.), it should be possible to understand these capture yields based on the thermodynamics of iodide-salt ion-pair formation in THF.

To explore this relationship, we examine how the electron-capture yields we observe vary with the ion-pair and free-ion distributions determined from conductivity measurements of salts in THF. Szwarc and coworkers have measured the conductivity of various cations in THF and other ethers over a range of temperatures and salt concentrations and found that salt dissociation constants for alkali cations are typically $\sim 10^{-5}$ M.[22,69–71] These workers also found that the solutions became highly non-ideal at concentrations above $\sim$100 μM, such that the fraction of the dissolved salt that is ion-paired saturates at $\sim$90% in the mM concentration range. This $\sim$90% pairing of sodium salts in the concentration range of our experiments is in striking agreement with the $\sim$90% electron-capture yield we observed in our NaI CTTS experiments (Fig. 3). On the other hand, pulse radiolysis experiments have determined that Na^+ cations are able to capture excess electrons with a 100% yield on the nanosecond time scale. Thus, the $\sim$10% of electrons that are not captured in the first 500 ps following CTTS excitation of Na^+-I^- in THF likely corresponds to the fraction of salt that was not initially ion-paired. Our observation that the capture yield did not change with salt concentration in the mM concentration range is also consistent with the known saturation of ion-pairing of other sodium salts in THF.[69]

In contrast to Na^+-I^- pairs, the relatively small blueshift of the CTTS transition of $t-BA^+$ iodide in THF, along with the low electron-capture yield we observed following the CTTS excitation of this salt (Fig. 5), suggests a significantly larger initial ion-pair separation. Surprisingly, however, Szwarc's conductivity studies indicate a similar degree of ion-pairing for $t-BA^+$ salts as for Na^+ salts in THF.[22] Based on conductivity data alone, we might have predicted a substantial fraction of electron capture by $t-BA^+$. We see two possibilities to explain the lack of spectral dynamics we observed on the hundreds-of-picoseconds time scale following CTTS excitation of $t-BA^+$ iodide (Fig. 5): either all of the ejected electrons are preferentially ejected within ∼1 solvent shell of the $t-BA^+$ cation following CTTS excitation (so that none are available to be diffusively captured on time scales longer than ∼5 ps) and only a small fraction are observed to be captured, or alternatively, electrons are ejected to a large average distance from the $t-BA^+$ cation and only the small fraction of electrons that happen to localize nearby a $t-BA^+$ are captured with high probability to form LCPs. These scenarios cannot be distinguished from the data in Fig. 5. However, in Section III B 2, we argued in conjunction with Fig. 4 that the tightly binding Na^+ cation alters the average I^- CTTS electron ejection distance from ∼6 nm to ≤ 2 nm, and it seems unlikely that the more weakly interacting $t-BA^+$ cation could cause an even greater contraction of the ejection distribution. Thus, we believe that $t-BA^+$ is unable to alter significantly the 'free' I^- CTTS electron-ejection distribution, such that LCPs are formed only by those electrons that happen to be ejected close to the $t-BA^+$ cations. Logically, the degree to which the CTTS excited state in the parent-I^- solvent cavity is able to nonadiabatically couple to the disjoint cavities that naturally exist in liquid THF depends on the proximity of the counterion: the more a cation is able to perturb the CTTS spectrum, the more likely it is to significantly alter the CTTS ejection distribution, and thus, the more likely it is to be able to capture the ejected electrons. Additionally, it is important to note that although the conductivity measurements reflect significant ion-pairing in both the Na^+ and $t-BA^+$ cases, these measurements tell us nothing about the shape (depth or position of the minimum) of the mean-force potential that binds the ion-pair together.

In summary, we have studied the effects of the counterion on the ultrafast CTTS dynamics of I^- in weakly-polar liquid THF. By switching counterions from crown-ether-complexed Na^+ to $t-BA^+$ to Na^+, we have been able to tune the degree of interaction with the I^- ion from essentially none to weak to strong, respectively. We found that depending on the degree

to which the ions initially interact, the counterion not only can alter the distance to which CTTS electrons are ejected but also can participate in the the CTTS process by capturing a significant fraction of the ejected electrons to form either tight or loose cation:electron contact pairs. Our previous work showed that when there is no significant interaction between I^- and its counterion in THF, CTTS excitation of I^- led to electron ejection with a ∼6 nm average ejection distance.[8] In contrast, for strongly ion-paired Na^+-I^-, we found that ∼90% of the CTTS-ejected electrons were captured by the Na^+ counterion to form tight-contact pairs within ∼100 ps, and a diffusion-based argument suggests that the average separation of Na^+-e^- pairs must be ≤ 2 nm. Thus, not only does the pairing with the Na^+ cation cause a significant blue-shift of the I^- CTTS spectrum, it also causes a profound contraction of the CTTS electron-ejection distribution. This contraction of the CTTS electron-ejection distribution, however, is not simply a coulombic effect: even though conductivity data suggests the degree of ion-pairing of Na^+ and $t-BA^+$ with I^- is similar, we found that only ∼10-15% of the CTTS-ejected electrons were captured by tetrabutylammonium cations to form loose-contact pairs. It appears that association with $t-BA^+$ does not significantly alter the CTTS electron-ejection distribution relative to 'free' I^-, a result that is likely a direct consequence of the fact that the initial separation of the $t-BA^+$-I^- ion-pair is relatively large, but may also be a reflection of the different chemical character of $t-BA^+$ relative to Na^+. Finally, our data also show that the kinetics of electron capture by Na^+ and $t-BA^+$ are significantly different: the rapid formation of weakly-interacting $(t-BA^+, e^-)_{THF}$ LCPs is likely to be barrierless, as implied by the 'ionic-solvation' model, whereas the slower formation of strongly-interacting $(Na^+, e^-)_{THF}$ TCPs appears to take place via interconversion from a more rapidly formed LCP; we will examine the Na^+-e^-_{THF} LCP→TCP interconversion in greater detail in an upcoming publication.[50]

V. ACKNOWLEDGEMENTS

This research was funded by the National Science Foundation under grant number CHE-0603766. The authors thank Dr. Ross E. Larsen and Molly C. Cavanagh for useful discussions.

APPENDIX A: INCORPORATING GROUP VELOCITY MISMATCH INTO ULTRAFAST KINETIC MODELS

When fitting kinetic models to the absorption transients associated with CTTS ejection from I^- salts in THF, it was necessary to account for a temporal response limited by the group-velocity mismatch (GVM) between the pump and probe pulses in our relatively thick samples (in addition to the usual finite resolution that results from temporal cross-correlation of the pump and probe pulses). This appendix describes the mathematical procedures we used to account properly for these effects on the ultrafast absorption transients. We will focus most of our attention on models that assume the underlying transient absorption dynamics, $I(t)$, can be expressed as a linear combination of exponentials:

$$I(t) = \sum_n A_n \exp\{-t/\tau_n\}. \tag{A1}$$

This is exactly the situation for the model we presented in Section III B to describe $(Na^+, e^-)_{THF}$ TCP formation following the CTTS excitation of NaI/THF solutions. As shown below, convolution of GVM effects with such a model is analytically tractable; we also outline a generic numerical procedure applicable to kinetic models with more complicated time dependence.

In the absence of a dispersive medium, the 'zero of time,' t_0, occurs when the optical path lengths (OPL) traveled by the pump and probe pulses are identical; the temporal pump-probe delay is then defined as $t = (\mathrm{OPL}_{pr} - \mathrm{OPL}_{pu})/c$, where c is the speed of light. When the pump and probe pulses travel through a dispersive medium such as a liquid sample, however, the optical path lengths are altered by the index of refraction of that medium. Thus, after penetrating a distance x into a dispersive medium, the 'zero of time' is shifted to $t_0(x) = t_0 + \Delta n_{pr-pu} x/c$, where $\Delta n_{pr-pu} = n_{pr} - n_{pu}$ is the difference in refractive index in the medium between the probe and pump pulses. As a result, the absorption transient originating at the penetration depth x in the medium begins from this shifted zero of time:

$$I_x(t - t_0(x)) = I_x(t - t_0 - \Delta n_{pr-pu} x/c). \tag{A2}$$

Since the zero of time changes as a function of x, the time-dependent signal measured in a pump-probe experiment is a convolution of the individual signal contributions at each x

across the sample depth:

$$I_{GVM}(t) = \int_0^{L(t)} I_x(t - t_0(0) - \Delta n_{pr-pu} x/c) \cdot w(x) dx, \tag{A3}$$

in which $w(x)$ is the weight of the contribution from each possible sample penetration depth, and for a sample medium of thickness D, $L(t) = ct/|\Delta n|$ if it is less than D, otherwise $L(t) = D$. To best mimic the experimental conditions, we have assumed that the sample-depth-dependent weighting of the x-dependent transients to the total signal is given by Beer's Law:

$$w(x) = \exp\{-\alpha_{pu} x\} / \int_0^D \exp\{-\alpha_{pu} x\} dx, \tag{A4}$$

where α_{pu} is the optical absorption of the sample at the pump wavelength and the overall weight is normalized for the finite depth of the sample.

To develop an analytic expression for the GVM-affected pump-probe transients, we must consider the sign of Δn_{pr-pu}. The most-common case encountered experimentally is when the pump pulse is retarded relative to the probe pulse upon passing through the medium (*i.e.*, $\Delta n_{pr-pu} < 0$); we will refer to this case as 'normal' GVM. In this 'normal' case, substitution of Eqs. A1, A2 and A4 into Eq. A3 yields an analytic solution to the convolution of the dispersive sample response with the multi-exponential population kinetics:

$$I_{GVM}(t) = \sum_n A_n \left[\frac{\tau^+_{inv,n}}{\tau_{GVM}}\right] \exp\{-t/\tau_n\} \left[\frac{1 - \exp\left\{-T(t)/\tau^+_{inv,n}\right\}}{1 - \exp\left\{-\tau_{cell}/\tau_{GVM}\right\}}\right], \tag{A5}$$

where $\tau_{cell} = |\Delta n_{pr-pu}| D/c$, $\tau_{GVM} = |\Delta n_{pr-pu}|/(\alpha_{pu} c)$, $T(t) = t$ if $t < \tau_{cell}$ but τ_{cell} otherwise, and $\left(\tau^+_{inv,n}\right)^{-1} = \tau^{-1}_{GVM} + \tau^{-1}_n$. If we further assume that the pump-probe cross-correlation is Gaussian with a full-width-at-half-maximum of $2\sigma\sqrt{\ln 2}$, then we can perform an additional convolution to account for the finite duration of the pump and probe pulses and obtain an analytic expression for the total signal:

$$\begin{aligned} S(t) = & \sum_n \frac{A_n \left[\tau^+_{inv,n}/\tau_{GVM}\right]}{2\left[1 - \exp(-\tau_{cell}/\tau_{GVM})\right]} \\ & \cdot \left[\exp\left(-\frac{t}{\tau_n} + \frac{\sigma^2}{4\tau_n^2}\right) \operatorname{erfc}\left(-\frac{t}{\sigma} + \frac{\sigma}{2\tau_n}\right)\right. \\ & + \exp\left(-\frac{t}{\tau_{n'}} + \frac{\sigma^2}{4\tau_{n'}^2}\right) \left[\operatorname{erfc}\left(\frac{\tau_{cell}}{\sigma} - \frac{t}{\sigma} + \frac{\sigma}{2\tau_{n'}}\right) - \operatorname{erfc}\left(-\frac{t}{\sigma} + \frac{\sigma}{2\tau_{n'}}\right)\right] \\ & \left. - \exp\left(-\frac{\tau_{cell}}{\tau^+_{inv,n}}\right) \exp\left(-\frac{t}{\tau_n} + \frac{\sigma^2}{4\tau_n^2}\right) \operatorname{erfc}\left(\frac{\tau_{cell}}{\sigma} - \frac{t}{\sigma} + \frac{\sigma}{2\tau_n}\right)\right] \end{aligned} \tag{A6}$$

in which $(\tau_{n'})^{-1} = (\tau_n)^{-1} + (\tau_{GVM})^{-1}$ and erfc(x) is the complementary error function. Equation A6 (with $n = 3$) is the analytic form that was fit to the Na^+-I^- CTTS/electron capture data in Fig. 3 using a non-linear least-squares procedure in order to obtain the fitting parameters $\{A_n, \tau_n\}$ (with τ_1 constrained to 380 fs) reported in Section III B.

It is also possible that $\Delta n_{pr-pu} > 0$, such that the probe pulse is retarded relative to the pump pulse upon entering the medium, a case that we refer to as 'anomalous' GVM. In this 'anomalous' case, the analytic solution to $I_{GVM}(t)$ obtained in Eq. A5 retains the same general form but with the substitutions $\tau^+_{inv,n} \rightarrow \tau^-_{inv,n}$, $\left(\tau^-_{inv,n}\right)^{-1} = (\tau_{GVM})^{-1} - (\tau_n)^{-1}$, and $\tau_{n'} \rightarrow \tau_{GVM}$. As a result of the sign change, a discrete singularity is introduced in this case when $\tau_n = \tau_{GVM}$, where the analytic expression for component n must be obtained by taking limits:

$$\begin{aligned} &I_{GVM,n}(t; \tau_n = \tau_{GVM}) = \\ &\frac{A_n}{[1 - \exp(-\tau_{cell}/\tau_{GVM})]} \cdot \frac{t}{\tau_{GVM}} \cdot \exp\left(-\frac{t}{\tau_{GVM}}\right) \text{ if } t \leq \tau_{cell}, \\ &\frac{A_n}{[1 - \exp(-\tau_{cell}/\tau_{GVM})]} \cdot \frac{\tau_{cell}}{\tau_{GVM}} \cdot \exp\left(-\frac{t}{\tau_{GVM}}\right) \text{otherwise.} \end{aligned} \tag{A7}$$

The cross-correlation-convolved contribution from component n in this condition is thus,

$$\begin{aligned} &S_n(t; \tau_n = \tau_{GVM}) = \\ &\frac{A_n}{[1 - \exp(-\tau_{cell}/\tau_{GVM})]} \cdot \exp\left(-\frac{t}{\tau_n} + \frac{\sigma^2}{4\tau_n^2}\right) \cdot \left[\tau_{cell} \operatorname{erfc}\left(\frac{\tau_{cell}}{\sigma} - \frac{t}{\sigma} + \frac{\sigma}{2\tau_n}\right)\right. \\ &+ \left(t - \frac{\sigma^2}{2\tau_n}\right) \cdot \left[\operatorname{erfc}\left(\frac{\tau_{cell}}{\sigma} - \frac{t}{\sigma} + \frac{\sigma}{2\tau_{n'}}\right) - \operatorname{erfc}\left(-\frac{t}{\sigma} + \frac{\sigma}{2\tau_{n'}}\right)\right] \\ &\left.+ \frac{1}{\sqrt{\pi}} \cdot \left[\exp\left(-\left(-\frac{t}{\sigma} + \frac{\sigma}{2\tau_{n'}}\right)^2\right) - \exp\left(-\left(\frac{\tau_{cell}}{\sigma} - \frac{t}{\sigma} + \frac{\sigma}{2\tau_{n'}}\right)^2\right)\right]\right]. \end{aligned} \tag{A8}$$

which could be analytically fit to ultrafast transient absorption dynamics in the case of 'anamalous' GVM.

Of course, there are many situations in which the ultrafast absorption dynamics of a sample are not simply modeled by a linear combination of exponentials; the 'ionic-solvation' model that we applied to describe the ultrafast electron capture dynamics in t−BA^+- I^- solutions in Section III C is a prime example. In such cases, we must assume that the intrinsic sample absorption dynamics are given by

$$I(t) = \int_0^t \epsilon(t - t') \frac{dP}{dt'} dt' \Big/ \int_0^\infty \frac{dP}{dt} dt, \tag{A9}$$

where $\epsilon(t)$ and $P(t)$ are the time-dependent spectral dynamics and population kinetics of the transient absorber; from this form, $I(t)$ can be reduced to a simple kinetic expression if $\epsilon(t)$ is constant in time. To our knowledge, no analytic method exists for convoluting the GVM-induced temporal response with time-dependent spectral shifting; thus, we have taken a numerical approach. Since the GVM parameters that limit the temporal resolution are known experimentally, the GVM convolution can be applied to $I(t)$ through a standard matrix multiplication:

$$I_{GVM}(t) = \underline{\underline{A}}_{GVM} \cdot I(t). \tag{A10}$$

Here, $\underline{\underline{A}}_{GVM}$ is an $N \times N$ matrix, with N representing the number of time-steps (δt) that span the desired time scale. The rows of $\underline{\underline{A}}_{GVM}$ give the (asymmetric) weighting function in time that is associated with $w(x)$, but with zeros along the diagonal, such that the summation involved in the matrix multiplication may approximate integration. To incorporate this numeric convolution into a fitting routine, we computed the combined the kinetic and spectral dynamics ($I(t)$) on a linear time-grid (typically δt = 20 fs, N = 30,000 points) according to the desired model. A sparse $N \times N$ delay-dependent GVM convolution matrix ($\underline{\underline{A}}_{GVM}$) was generated once and stored in memory. Convolution was accomplished via Eq. A10, and $I_{GVM}(t)$ was then folded with the symmetric cross-correlation function using a simple numeric convolution algorithm. This procedure was then used iteratively in a 'forward-convolute-and-compare' scheme to minimize the fitting parameters; this is the procedure we employed to fit the 'ionic solvation' model to the $t-\mathrm{BA}^{+}$-I^{-} data presented in Section III C.

---

* Electronic mail:schwartz@chem.ucla.edu

[1] Chen, X.; Bradforth, S. E. *Annu. Rev. Phys. Chem.* **2008**, *59*, 203.

[2] Blandamer, M. J.; Fox, M. F. *Chem. Rev.* **1970**, *70*(1), 59–93.

[3] Vilchiz, V. H.; Chen, X.; Kloepfer, J. A.; Bradforth, S. E. *Radiat. Phys. Chem.* **2005**, *72*(2-3), 159–167.

[4] Kloepfer, J. A.; Vilchiz, V. H.; Lenchenkov, V. A.; Germaine, A. C.; Bradforth, S. E. *J. Chem. Phys.* **2000**, *113*(15), 6288–6307.

[5] Vilchiz, V. H.; Kloepfer, J. A.; Germaine, A. C.; Lenchenkov, V. A.; Bradforth, S. E. *J. Phys. Chem. A* **2001**, *105*(10), 1711–1723.

[6] Xia, C.-G.; Peon, J.; Kohler, B. *J. Chem. Phys.* **2002**, *117*(19), 8855–8866.

[7] Iglev, H.; Trifonov, A.; Thaller, A.; Buchvarov, I.; Fiebig, T.; Laubereau, A. *Chem. Phys. Lett.* **2005**, *403*(1-3), 198–204.

[8] Bragg, A. E.; Schwartz, B. J. *J. Phys. Chem. B* **2008**, *112*, 483–494.

[9] Barthel, E. R.; Martini, I. B.; Schwartz, B. J. *J. Chem. Phys.* **2000**, *112*(21), 9433–9444.

[10] Barthel, E. R.; Martini, I. B.; Schwartz, B. J. *J. Phys. Chem. B* **2001**, *105*(49), 12230–12241.

[11] Barthel, E. R.; Martini, I. B.; Keszei, E.; Schwartz, B. J. *J. Chem. Phys.* **2003**, *118*(13), 5916–5931.

[12] Barthel, E. R.; Schwartz, B. J. *Chem. Phys. Lett.* **2003**, *375*(3-4), 435–443.

[13] Martini, I. B.; Barthel, E. R.; Schwartz, B. J. *J. Chem. Phys.* **2000**, *113*(24), 11245–11257.

[14] Wang, Z.; Shoshana, O.; Hou, B.; Ruhman, S. *J. Phys. Chem. A* **2003**, *107*(17), 3009–3016.

[15] Shoshana, O.; Pérez Lustres, J. L.; Ernsting, N. P.; Ruhman, S. *Phys. Chem. Chem. Phys.* **2006**, *8*(22).

[16] In acetonitrile clusters, some solvated electrons react with the unsaturated solvent molecules to form valence-bound motifs,[72,73] which also has been observed in solution following CTTS excitation of I^- in acetonitrile.[6].

[17] Bedard-Hearn, M. J.; Larsen, R. E.; Schwartz, B. J. *J. Chem. Phys.* **2005**, *122*(13), 134506.

[18] Bowron, D. T.; Finney, J. L.; Soper, A. K. *J. Am. Chem. Soc.* **2006**, *128*(15), 5119–5126.

[19] Bedard-Hearn, M. J.; Larsen, R. E.; Schwartz, B. J. *J. Chem. Phys.* **2006**, *125*, 194509.

[20] Martini, I. B.; Barthel, E. R.; Schwartz, B. J. *Science* **2001**, *293*(5529), 462–465.

[21] There are some monovalent salts that are well-known exceptions: for instance, AgI.

[22] Nicholls, D.; Sutphen, C.; Szwarc, M. *J. Phys. Chem.* **1968**, *72*(3), 1021.

[23] Blandamer, M. J.; Gough, T. E.; Symons, M. C. R. *Trans. Faraday Soc.* **1966**, *62*(518P), 286.

[24] Sciaini, G.; Marceca, E.; Fernandez-Prini, R. *J. Phys. Chem. B* **2005**, *109*(40), 18949–18955.

[25] Sciaini, G.; Marceca, E.; Fernandez-Prini, R. *J. Supercrit. Fluids* **2005**, *35*(2), 106–110.

[26] Sciaini, G.; Marceca, E.; Fernandez-Prini, R. *Phys. Chem. Chem. Phys.* **2006**, *8*(42), 4839–4848.

[27] Sciaini, G.; Marceca, E.; Fernandez-Prini, R. *J. Phys. Chem. B* **2006**, *110*(18), 8921–8923.

[28] Stein, G.; Treinin, A. *Trans. Faraday Soc.* **1960**, *56*, 1393.

[29] Sauer, M. C.; Shkrob, I. A.; Lian, R.; Crowell, R. A.; Bartels, D. M.; Chen, X.; Suffern, D.;

Bradforth, S. E. *J. Phys. Chem. A* **2004**, *108*(47), 10414–10425.

[30] Anbar, M.; Hart, E. J. *J. Phys. Chem.* **1965**, *69*.

[31] Gelabert, H.; Gauduel, Y. *J. Phys. Chem.* **1996**, *100*(33), 13993–14004.

[32] Mizuno, M.; Tanaka, J.; Harada, I. *J. Phys. Chem.* **1981**, *85*(13), 1789–1794.

[33] Banin, U.; Ruhman, S. *J. Chem. Phys.* **1993**, *98*(6), 4391–4403.

[34] Bragg, A. E.; Schwartz, B. J. in preparation, **2007**.

[35] This observation is consistent with published K_{diss} values determined from conductivity measurements with other alkali salts in THF:[22,69,70] ion-pair 'saturation' is approached in the millimolar concentration range. Dissolution is favored at concentrations well below 1 mM, well below the range we can study currently with our time-resolved experiments.

[36] Nguyen, T.-Q.; Martini, I. B.; Liu, J.; Schwartz, B. J. *J. Phys. Chem. B* **2000**, *104*(2), 237–255.

[37] Tauber, M. J.; Mathies, R. A.; Chen, X.; Bradforth, S. E. *Rev. Sci. Inst.* **2003**, *74*.

[38] This means that, in samples that did not strongly absorb the pump light, our effective time resolution is only on the order of ∼1 ps.

[39] Jou, F.-Y.; Dorfman, L. M. *J. Chem. Phys.* **1973**, *58*(11), 4715–4723.

[40] Jou, F.-Y.; Freeman, G. R. *Can. J. Chem.* **1976**, *54*(23), 3693–3704.

[41] Dorfman, L. M.; Jou, F.-Y.; Wageman, R. *Ber. Bunsen-Ges. Phys. Chem.* **1971**, *75*(7), 681.

[42] Jou, F.-Y.; Freeman, G. R. *Can. J. Chem.* **1979**, *57*(5), 591–597.

[43] Bockrath, B.; Dorfman, L. M. *J. Phys. Chem.* **1973**, *77*(8), 1002–1006.

[44] Seddon, W. A.; Salmon, G. A.; Fletcher, J. W. *Radiat. Res.* **1974**, *59*(1), 111–111.

[45] Klooster, J. G.; Giling, L. J.; Rettschn, R. P.; Vanvoors, J. D. *Chem. Phys. Lett.* **1971**, *8*(5), 462.

[46] Renou, F.; Mostafavi, M.; Archirel, P.; Bonazzola, L.; Pernot, P. *J. Phys. Chem. A* **2003**, *107*(10), 1506–1516.

[47] Renou, F.; Archirel, P.; Pernot, P.; Levy, B.; Mostafavi, M. *J. Phys. Chem. A* **2004**, *108*(6), 987–995.

[48] Renou, F.; Pernot, P.; Bonin, J.; Lampre, I.; Mostafavi, M. *J. Phys. Chem. A* **2003**, *107*(34), 6587–6593.

[49] Cavanagh, M. C.; Larsen, R. E.; Schwartz, B. J. *J. Phys. Chem. A* **2007**, *111*(24), 5144–5157.

[50] Bragg, A. E.; Cavanagh, M. C.; Schwartz, B. J. **2007**.

[51] Seddon, W. A.; Fletcher, J. W.; Catterall, R.; Sopchyshyn, F. C. *Chem. Phys. Lett.* **1977**,

48(3), 584–586.

[52] Seddon, W. A.; Fletcher, J. W.; Sopchyshyn, F. C.; Catterall, R. *Can. J. Chem.* **1977**, *55*(19), 3356–3363.

[53] Catterall, R.; Slater, J.; Symons, M. C. R. *J. Chem. Phys.* **1970**, *52*(2), 1003.

[54] We note, however, that the 1080-nm transient does exhibit non-isosbestic behavior at earlier delays (Fig. 3(l)), indicating that the fastest dynamics cannot be understood in terms of simple two-state kinetics.

[55] We do not have an independent measurement of the free-electron/TCP branching ratio on the 1-ns time scale, and must rely on the kinetics of these transients to determine this value.

[56] The stoichiometry of the initial CTTS reaction, Eq. 3a, mandates that the population of the CTTS-excited state, I^{-*}, decays with the same rate constant, k_{CTTS}, at which the e^- and neutral iodine atom appear. As no spectroscopic signatures of I^{-*} or I have ever been observed at the wavelengths examined here, we neglect their population dynamics in this analysis.

[57] Blandamer *et al.* have argued that the substantial shift of the alkali-iodide transition from its (molecular) gas-phase charge-transfer-to-cation (CTTC) transition (at 30,000 cm^{-1}) to the 42,600-cm^{-1} transition measured in THF could not arise simply from dipole solvation of a contact-ion pair, and suggested that the alkali-iodide salts should exist as solvent-separated ion pairs in THF, such that the solvent breaks the molecular character of the pair.[23] More recently, Sciaini *et al.*[26] concluded that the iodide-salt absorption band associated with contact ion-pairs in SCA does not have molecular CTTC character: since the cation is strongly coordinated by local solvent molecules, this band is described best as a perturbed I^- CTTS transition. These interpretations are consistent with our conclusion in Section III B 2 that UV excitation of Na^+-I^- in THF does not promote direct CTTC due to an appreciable solvent barrier.

[58] Smoluchowski, M. *Z. Phys. Chem.* **1917**, *92*, 129.

[59] Rice, S. A. *Diffusion-Limited Reactions*, Vol. 25 of *Chemical Kinetics;* Elsevier, 1985.

[60] Green, N. J. B. *Chem. Phys. Lett.* **1984**, *107*(4-5), 485–488.

[61] Green, N. J. B.; Pilling, M. J.; Clifford, P. *Mol. Phys.* **1989**, *67*(5), 1086–1097.

[62] Clifford, P.; Green, N. J. B.; Pilling, M. J. *J. Phys. Chem.* **1982**, *86*, 1318.

[63] Clifford, P.; Green, N. J. B.; Pilling, M. J. *J. Phys. Chem.* **1984**, *88*(18), 4171–4176.

[64] Some evidence suggests that the THF radical cation undergoes rapid chemistry with other solvent molecules after MPI,[13] so that the electron may later combine with a radical that was

not from the original parent, as is the case for the multiphoton ionization of water.[63,74].

[65] The mobility of e^-_{THF}, μ, has been measured as $3 \cdot 10^{-3}\,\mathrm{cm}^2/\mathrm{Vs}$.[75] The e^-_{THF} diffusion constant, D, has been calculated[13] using Einstein's relation, $D = (k_B T/e)\mu$, in which e is the elementary charge, T is room temperature, and k_B is Boltzmann's constant.

[66] Independent conductivity measurements in THF suggest that cation-solvent interactions will limit the Na^+ diffusion rate.[70].

[67] Given the difficulty associated with collimating and aligning IR beams at these wavelengths, much of this small long-time decay ($\leq 3\%$) may be due to experimental artifacts such as misalignment of the translation stage; it is also possible that this small decay represents the onset of diffusion-limited chemical reactions (scavenging, etc.) with impurities in the solution.

[68] Substantial deviation from the Lorentzian lineshape occurs at higher energies. The high-energy tail is dominated by transitions to higher-lying excited disjoint states, as determined from recent MD simulations.[17].

[69] Chang, P.; Slates, R. V.; Szwarc, M. *J. Phys. Chem.* **1966**, *70*(10), 3180.

[70] Bhattacharyya, D. N.; Smid, J.; Szwarc, M. *J. Phys. Chem.* **1964**, *69*(2), 608.

[71] Although the conductivity experiments in refs. 70 69, and 22 studied alkali and tetrabutylammonium salts of aromatic radical anions in THF, we anticipate that the dissociation of corresponding iodide salts should not be significantly different.

[72] Mitsui, M.; Ando, N.; Kokubo, S.; Nakajima, A.; Kaya, K. *Phys. Rev. Lett.* **2003**, *91*(15), 153002.

[73] Shkrob, I. A.; Takeda, K.; Williams, F. *J. Phys. Chem. A* **2003**, *106*(39), 9132.

[74] Goulet, T.; Jay-Gerin, J.-P. *J. Chem. Phys.* **1992**, *96*, 5076.

[75] Dodelet, J.-P.; Freeman, G. R. *Can. J. Chem.* **1975**, *53*, 1263.

FIG. 1: Steady-state absorption spectra of the lowest-energy I^- CTTS transition in different solvents and counterion environments, normalized at the peak absorption for ease of comparison. Decreasing the polarity by switching from H_2O ($\epsilon = 78$, black curve) to THF ($\epsilon = 7.5$, red squares) produces a significant red-shift of the 'counterion-free' I^- CTTS transition: the CTTS λ_{max} shifts from 225 nm in water to 254 nm in THF. We obtained the CTTS spectrum of 'counterion-free' I^- in THF by chelating Na^+ with 18-crown-6 ether; see Ref. 8. In low-polarity THF, the choice of counterion can also shift the I^- CTTS transition energy due to specific ion-pairing interactions: the I^- CTTS transition with weakly associated $t-BA^+$ (green circles) has its λ_{max} at 248 nm, whereas the more strongly-associated Na^+ (blue diamonds) shifts the λ_{max} to 236 nm.

FIG. 2: The spectroscopy of solvated electrons and cation-electron complexes in THF. The room temperature spectra of e^-_{THF} (red squares) and $(Na^+, e^-)_{THF}$ (blue diamonds) were obtained from Refs. 39 and 43, respectively; the room temperature spectrum of $e^-_{H_2O}$ (black curve, Ref. 42) is included for reference. The $(Na^+, e^-)_{THF}$ species has been identified as a tight-contact pair (TCP) with partially atomic character. In contrast, solvated electrons in the presence of partially coordinated Na^+ (which are obtained, for example, by solvating Na^+ in polyglycoldimethyl ethers) gives rise to 'loose-contact-pairs' (LCPs), which are characterized by a coulombically induced blue-shift of the free solvated electron's spectrum (see Ref. 51). As discussed in Section III C, we see a similar LCP species formed following the CTTS ejection of an electron from I^- in the presence of $t-BA^+$. The spectrum of this species (green dashed curve) was obtained from fits to data plotted in Fig. 5 subject to the 'ionic-solvation' model described in the text.

FIG. 3: Absorption transients measured at selected IR wavelengths following the 263-nm excitation of NaI/THF solutions on both long (panels (a)-(g)) and short (panels (h)-(n)) time scales; the transients have been normalized at $t = 25$ ps for ease of comparison. The induced absorption at long IR wavelengths (1670, 1440, 1270, 1185 nm) decreases over 10's-100's of ps and is accompanied by a concomitant absorption increase at shorter wavelengths (700 and 920 nm), with a relatively flat temporal response at 1080 nm. This behavior illustrates the reaction of $e^-_{\rm THF}$ with Na^+ to form a $(Na^+, e^-)_{\rm THF}$ tight-contact pair (*cf.* Fig. 2, blue diamonds). The black curves are a global fit to all 7 transients using a simple, two-time-scale kinetic model described in the text. According to this model, 63 ± 3 and 26 ± 3 % of the CTTS-ejected electrons are captured by Na^+ to form TCPs with 2.3 ± 0.6 and 63 ± 15 ps lifetimes, respectively; ∼11 % of injected electrons remain as free $e^-_{\rm THF}$. The poor quality of the fit at intermediate wavelengths (*e.g.*, 1185 and 1080 nm) suggests that dynamic solvation processes that are not included in this model also are involved in the capture reaction.[50]

FIG. 4: Comparison of time-resolved absorption transients associated with $(Na^+, e^-)_{\rm THF}$ TCP formation following CTTS excitation of NaI in THF (blue diamonds), geminate recombination of $e^-_{\rm THF}$ with THF^+ following 263-nm multiphoton ionization (MPI) of THF at 263 nm (green circles), and geminate recombination following CTTS excitation of 'counterion-free' I^- in THF (red squares); all of the transients have been normalized at $t = 10$ ps. The (lack of) electron-I recombination in THF is well-modelled with a solution to the Smoluchowski equation for diffusion assuming a large (∼6 nm) initial electron-I separation (red solid curve), as supported by excited-state scavenging experiments (Ref. 8). In contrast, the recombination of $e^-_{\rm THF}$ with Na^+ and THF^+ is driven by conductive-diffusive motion of the electron-cation pair and is best modelled with solutions to the Debye-Smoluchowski equation (DSE). The green dashed curve is a DSE fit to the MPI recombination data with an initial separation (r_0) of 37 ± 2 Å when the reaction distance (R) and velocity (v) are fixed at 11 Å and 1.2 m/s, respectively (Refs. 8,13). The formation of $(Na^+, e^-)_{\rm THF}$ occurs more quickly, suggesting that the CTTS-generated electrons localize close to Na^+; the blue short-dashed curve is a DSE fit to the data with $r_0 = 24 \pm 3$ Å and $v = 6 \pm 2$ m/s holding R fixed at 11 Å. The large change in r_0 in the presence (24 Å) and absence (∼60 Å) of Na^+ illustrates that Na^+ either contracts spatial extent of the solvent cavity states coupled to the CTTS state or directly alters the nature of the I^- CTTS state.

FIG. 5: IR absorption transients measured after 263-nm CTTS excitation of tetrabutylammonium iodide in THF on long (panel (a)) and short (panel (b)) time scales; the transients have been normalized at $t = 40$ ps and offset vertically for clarity. Panel (a) demonstrates that the induced absorption decay is $\leq 3\%$ out to 1 ns, indicating that neither long-time geminate recombination nor significant electron capture occurs in these solutions. The short-time dynamics in panel (b) show a small absorption decay at red wavelengths with a corresponding rise at blue wavelengths, reflecting that a small fraction ($\sim$10-15%) of the electrons form $(t{-}\mathrm{BA}^+, e^-)_{\mathrm{THF}}$ loose-contact pairs (LCPs). The black curves are a global fit of all 10 transients to the 'ionic-solvation' model described in the text, which includes a continuous, time-dependent blue-shift of the electron spectrum as it is captured by $t{-}\mathrm{BA}^+$ to form the LCP. We also fit the data to a 'kinetic-capture' model similar to that used to describe the NaI data in Fig. 3; the fit to this model is visually indistinguishable from the fit to the 'ionic-solvation' model; the fitting parameters obtained using both models are summarized in Table I. The ionic-solvation model provides a slightly better numerical fit to the data, and the LCP spectrum obtained from this model is plotted as the green dashed curve in Fig. 2.

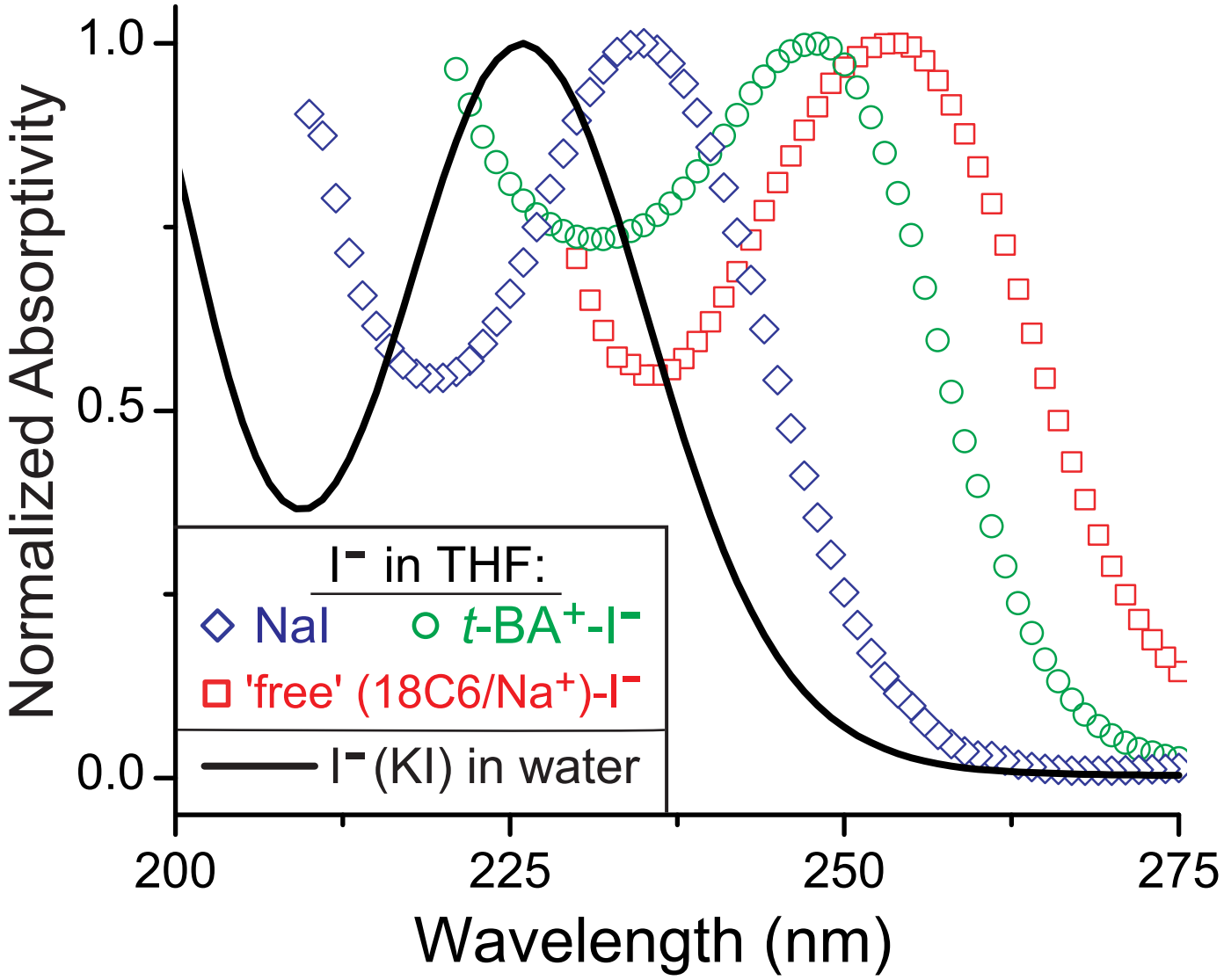

Bragg and Schwartz, Figure 1

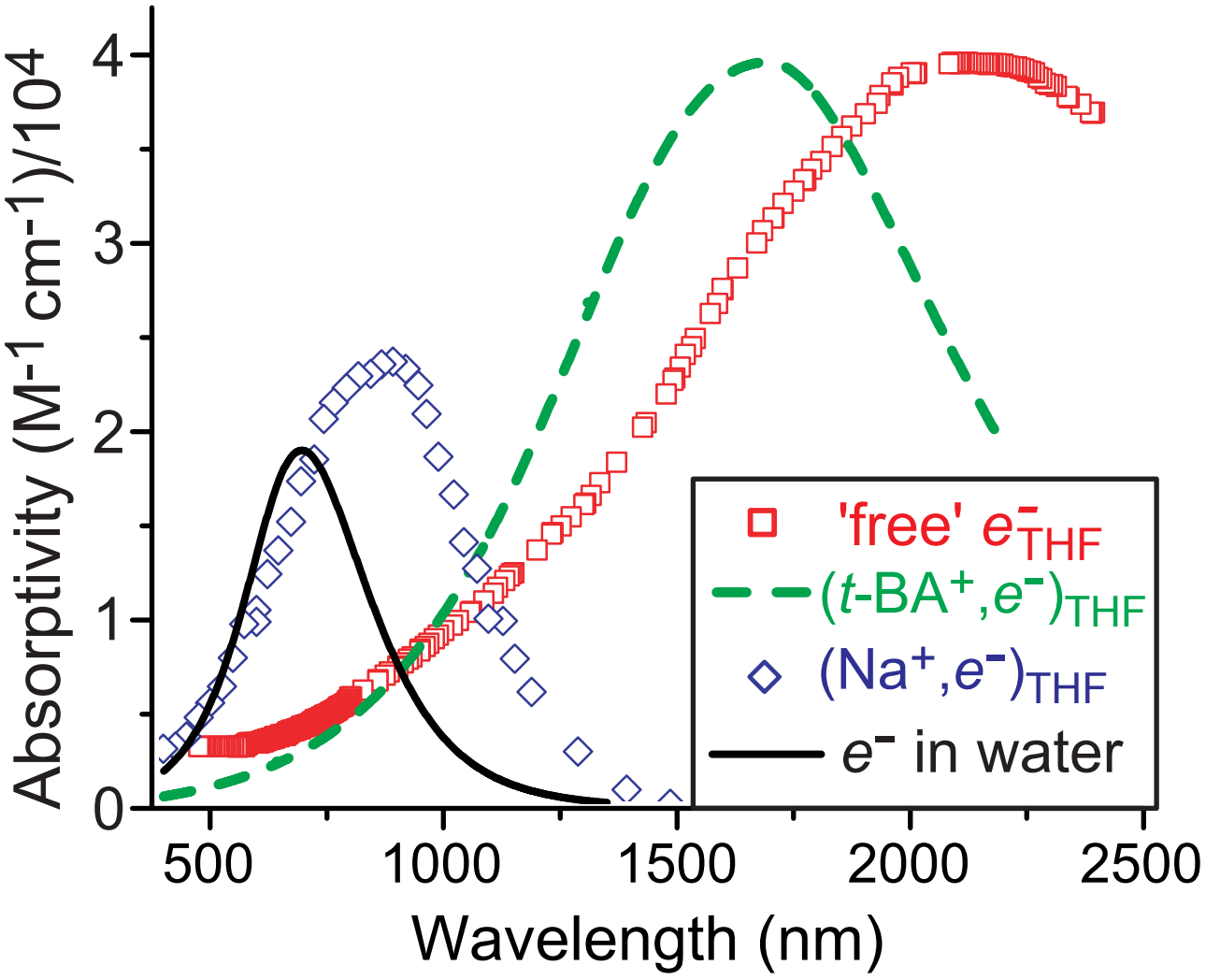

Bragg and Schwartz, Figure 2

Submitted to The Journal of Physical Chemistry

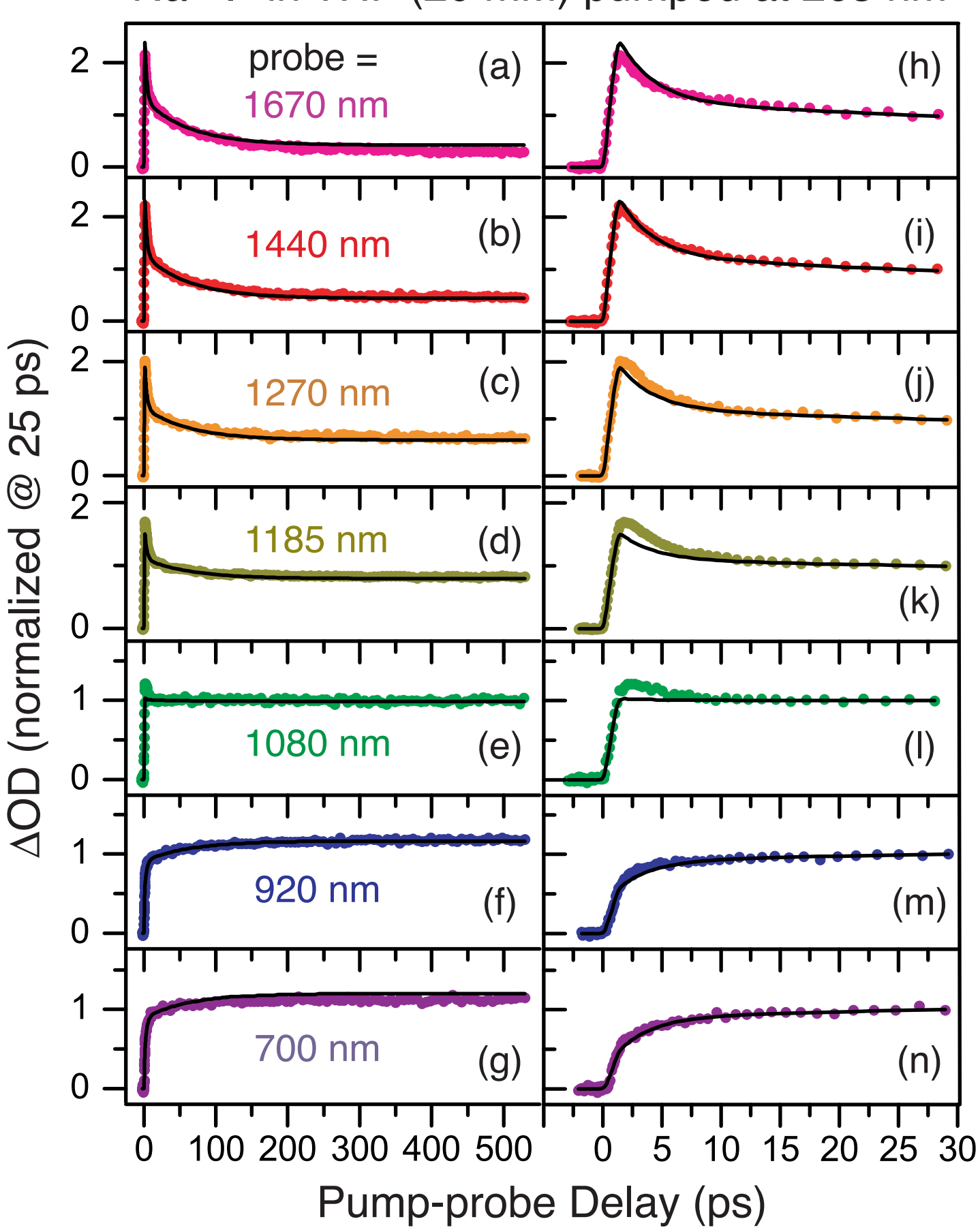

Bragg and Schwartz, Figure 3

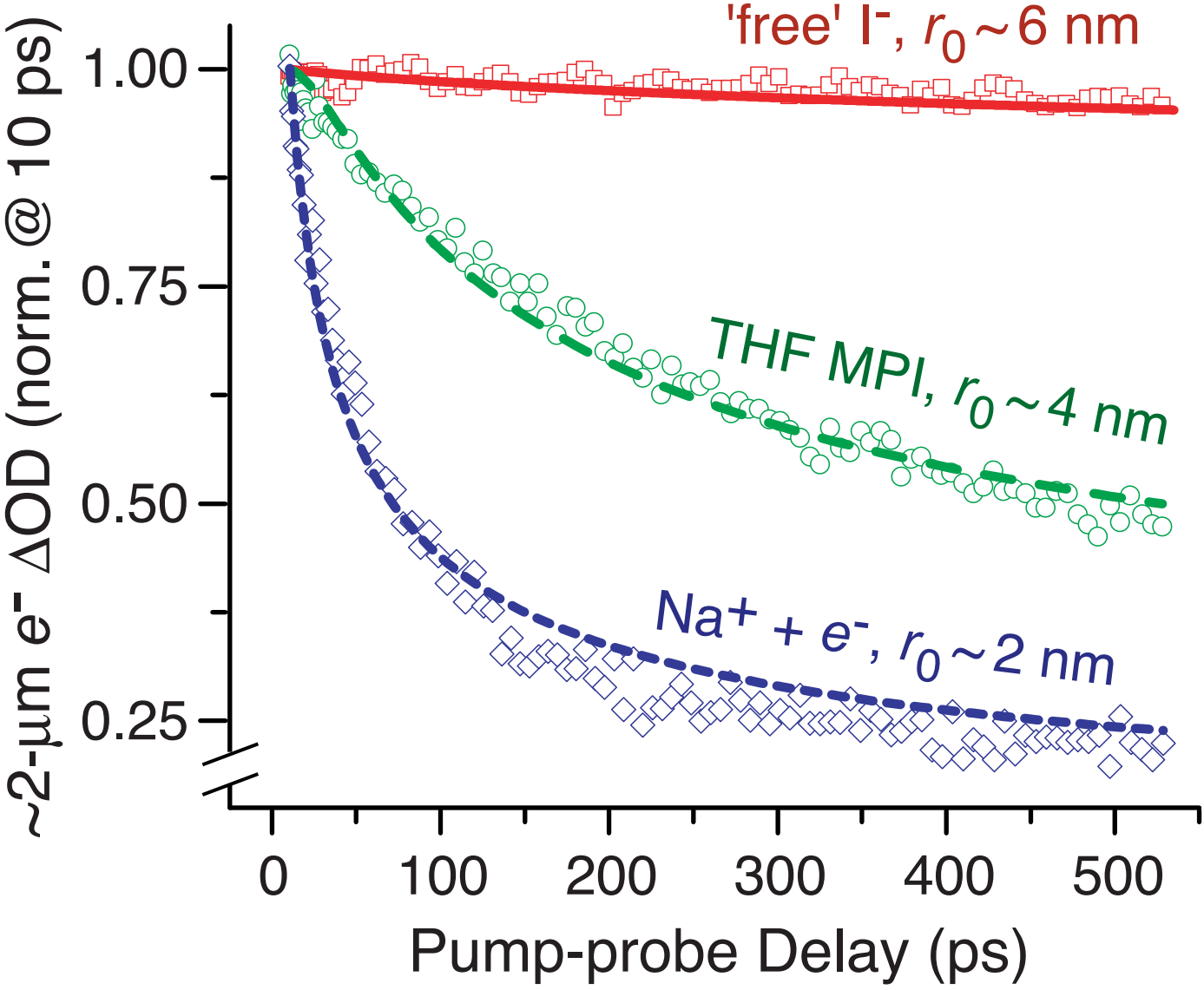

Bragg and Schwartz, Figure 4

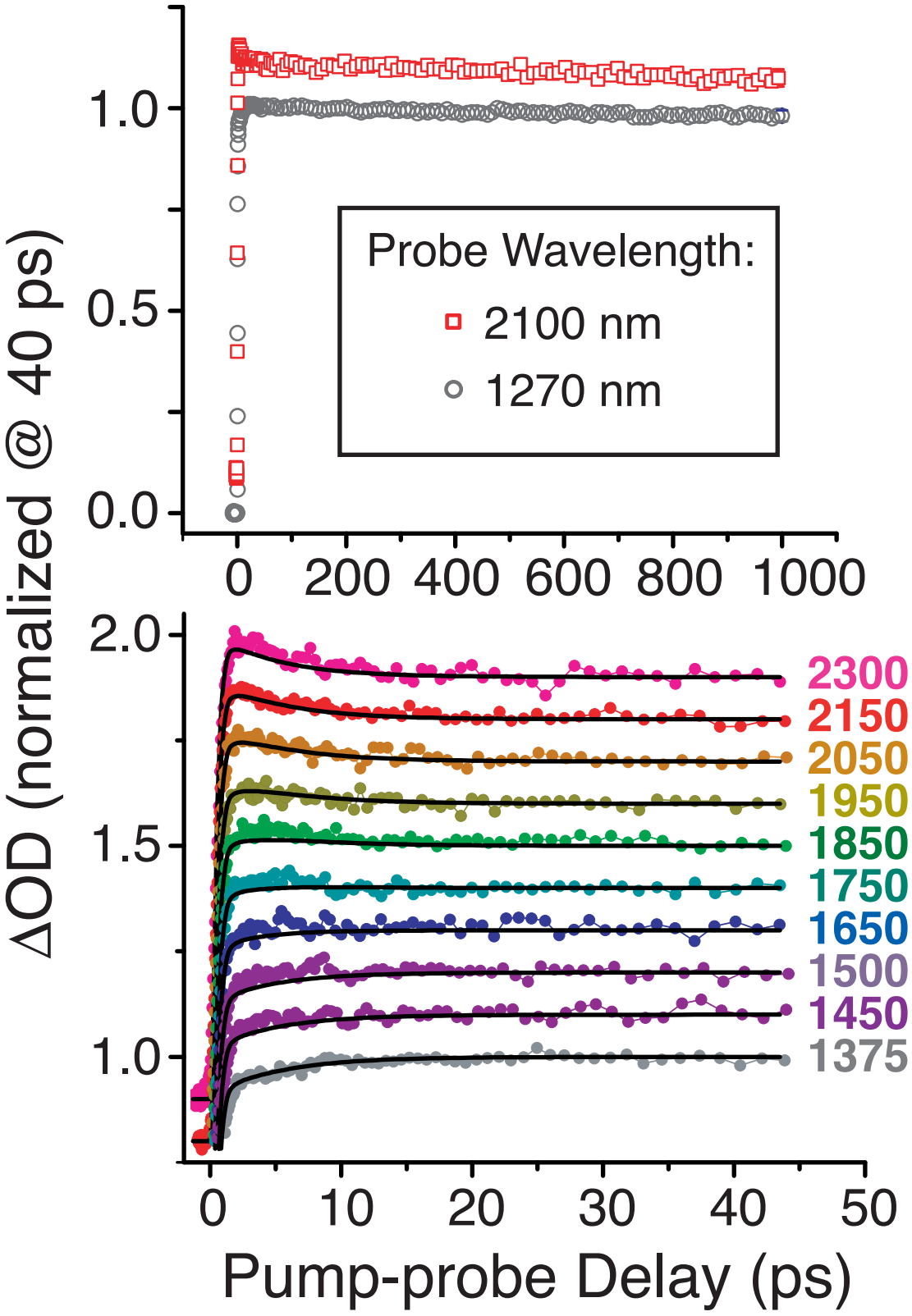

Bragg and Schwartz, Figure 5